國立臺灣大學工學院機械工程學系

碩士論文

Department of Mechanical Engineering

College of Engineering

National Taiwan University

Master's Thesis

載重車輛的即時狀態估測與參數識別

Real-time State Estimation and Parameter Identification of Load-carrying Vehicles Using a Dual Kalman Filter

楊宜瑄

Yi-Syuan Yang

指導教授：蘇偉儁 博士

Advisor: Wei-Jiun Su, Ph.D.

中華民國 113 年 7 月

July 2024

doi:10.6342/NTU202403171

Abstract

This research investigates the significance of state estimation, with a specific focus on parameter identification techniques, emphasizing its use in Advanced Driver Assistance Systems (ADAS). Through a comprehensive review of real-time estimation methods, including Kalman filtering and recent advancements, assessing their applicability, advantages, and limitations in relevant literature. The proposed approach utilizes a 4-degree-of-freedom vehicle model, incorporating the tire magic formula model and employing discretization techniques. The Dual Extended Kalman Filter (DEKF) framework is proposed as the primary estimation method, and is implemented using MATLAB/Simulink environment. The research justifies the use of dSPACE ASM as a surrogate for real-world testing, detailing test cases, sensor specifications, maneuvers, and their relevance to research objectives. Results demonstrate efficacy of the proposed methodology in parameter identification and its enhancing effect on vehicle state estimation accuracy across various maneuvers.

Keywords: Vehicle state estimation; Vehicle parameter estimation; Dual Extended Kalman filter;

doi:10.6342/NTU202403171

摘要

本研究旨在探討狀態估測以及參數識別對於車輛模型的重要性，強調其在加強先進駕駛輔助系統 (ADAS) 性能方面的作用。透過回顧相關文獻中即時估測的方法，包括卡爾曼濾波及其最新進展，本研究評估了這些方法的適用性、優點和局限性。研究中所提出演算法利用一個四自由度的車輛模型，結合 Magic Formula 輪胎模型，並採用了離散化空間狀態模型來進行狀態與參數估測。由於擴展卡爾曼濾波(EKF)具計算效率佳和適用於複雜系統等優點，因此以雙擴展卡爾曼濾波(DEKF)為框架設計估測演算法。此基於雙擴展卡爾曼濾波的估測方法於 MATLAB/ Simulink 環境中進行模擬。該研究模擬使用 dSPACE ASM 模擬軟體，以多體虛擬車輛替代實車測試。本篇研究中詳盡說明測試案例、感測器規格和過程中使用的模擬工況，以及它們與研究目標的相關性。模擬結果顯示，所提出的狀態與參數識別方法能夠改善車輛在不同情況下的狀態估測精度。

關鍵字: 車輛狀態估測；車輛參數估計；雙擴展卡爾曼濾波；

doi:10.6342/NTU202403171

Contents

doi:10.6342/NTU202403171

doi:10.6342/NTU202403171

doi:10.6342/NTU202403171

doi:10.6342/NTU202403171

doi:10.6342/NTU202403171

List of figures

doi:10.6342/NTU202403171

doi:10.6342/NTU202403171

doi:10.6342/NTU202403171

doi:10.6342/NTU202403171

List of tables

doi:10.6342/NTU202403171

Nomenclature

Symbols

a_x	Longitudinal acceleration at COG
a_y	Lateral acceleration at COG
b	Distance from COG to front axle
c	Distance from COG to rear axle
F_{xij}	Longitudinal force of wheel ij
F_{yij}	Lateral force of wheel ij
F_{zij}	Vertical force of wheel ij
$\mathrm{h_s}$	COG height from axle plane
I_x	Vehicle moment of inertia about x-axis
I_z	Vehicle moment of inertia about z-axis
l	Wheelbase
m	Total vehicle mass
m_s	Sprung vehicle mass
r	Wheel radius
s_{ij}	Slip ratio of tire ij
t_f	Front track width
t_r	Rear track width

doi:10.6342/NTU202403171

v_x	Longitudinal velocity at COG
v_y	Lateral velocity at COG
α_{ij}	Slip angle of tire ij
β	Vehicle body slip
β_ϕ	Roll damping
δ	Steering angle of front wheels
κ_{phi}	Roll stiffness
ψ	Vehicle yaw angle
$\dot{\psi}$	Vehicle yaw rate
Φ	Vehicle roll angle
$\dot{\phi}$	Vehicle roll rate

For all symbols, the subscript index ij refer to individual tires, specified as:

fl	Front right
fr	Front left
rl	Rear left
rr	Rear right

doi:10.6342/NTU202403171

Acronyms

ADAS	Advanced Driver Assistance Systems
AKF	Adaptive Kalman filter
COG	Center of Gravity
CR	Constant radius maneuver
DEKF	Dual extended Kalman filter
DLC	Double Lane Change Maneuver
EKF	Extended Kalman Filter
GNSS	Global navigation satellite system
GPU	Global positioning system
IMU	Inertial measurement unit
ISO	International Organization for Standardization
KF	Kalman filter
RLS	Recursive least squares
RMS	Root mean square
SAE	Society of Automotive Engineers
UKF	Unscented Kalman filter

doi:10.6342/NTU202403171

Chapter 1 Introduction

1.1 Introduction

With the development of intelligent vehicles and rapid growth of advanced driver assistance systems (ADAS), the importance of state estimation in vehicle control has become increasingly emphasized. Critical vehicle states include linear and angular position, velocity, and accelerations, as well as tire forces. States such as vehicle body slip and load transfer ratio, which cannot be directly measured, are derived from these primary states. Additionally, the center of gravity (COG) position and inertial properties are crucial for assessing vehicle performance. While this information can be obtained through measurements and is often provided by automotive manufacturers, it varies with different loading situations. Accurate and robust estimation of these vehicle states and parameters is essential for vehicle control systems and ADAS applications. Implementing a central estimation algorithm offers significant benefits, including conserving computational resources compared to individual estimations spread across different vehicle modules.

doi:10.6342/NTU202403171

1.2 Motivation

This research aims to develop an algorithm for real-time estimation of load-carrying vehicles, which typically have a higher center of mass and carry varying loads. Analysis of car accidents [1] indicates that vehicles with relatively higher centers of gravity, including vans and trucks, are more susceptible to rollovers compared to standard passenger vehicles. Although rollover accidents constitute a smaller portion of total accidents, they have a significantly higher fatality rate.

The motivation for this research is to improve robustness and accuracy of state estimation in vehicle control systems of such vehicles, facilitating the integration of ADAS, for example rollover prevention and stability control programs. As advanced vehicle technology rapidly evolves, there is a growing need to identify inertial parameters to enhance vehicle performance and safety. Consequently, exploration and evaluation of real-time estimation methods are particularly valuable for load-carrying vehicles.

By conducting a comprehensive review of state-of-the-art methods including Kalman filtering and recent advancements, this study aims to assess their practicality, advantages, and limitations, with a specific emphasis on parameter identification techniques. By employing a 4 degree-of-freedom (DOF) vehicle model, sophisticated tire modeling, and the Dual Extended Kalman Filter (DEKF)

doi:10.6342/NTU202403171

framework, this research highlights the complexity and critical importance of accurate state estimation in vehicle dynamics. The algorithm leverages readily available vehicle sensors, aiming to make state estimation more accessible and feasible for widespread adoption in the automotive industry. The state and parameter estimator proposed, designed for real-time execution, is built using MATLAB/Simulink and validated with a virtual vehicle platform (dSPACE ASM), facilitating its integration into existing vehicle control systems.

Ultimately, this research seeks to contribute to the advancement of vehicle control technology by providing insights into effective state estimation methodologies, thereby enhancing vehicle safety, efficiency, and performance across various driving conditions and maneuvers while emphasizing the importance of computational efficiency.

1.3 Organization of this Thesis

Chapter 2 provides a comprehensive literature review of previous developments in state estimation and inertia parameters, detailing foundational work and findings in this field. Chapter 3 introduces the Kalman Filter (KF) and its improved form, the Dual Extended Kalman Filter (DEKF), forming the foundation of the estimation algorithm presented. This chapter delves into the theoretical basics of this filtering

doi:10.6342/NTU202403171

technique. Chapter 4 presents an in-depth description of vehicle modeling, covering the dynamics of the vehicle body and the Magic Formula tire model. Chapter 5 outlines the simulation setup, discussing the test environment, vehicle specifications, and detailing the maneuvers used to validate the proposed algorithm. Chapter 6 presents the results and conclusions, analyzing the effectiveness of the proposed algorithm as a state estimation and parameter identification tool. Chapter 7 summarizes the findings and discusses their implications for the future of vehicle state estimation and parameter identification methods.

doi:10.6342/NTU202403171

Chapter 2 Literature Review

In modern vehicles, the integration of vehicle control systems has become increasingly common, making precise state estimation crucial for their efficiency and accuracy. For an estimator to perform effectively, it is also essential to identify the parameters that describe the vehicle's dynamics.

The states are dynamic variables that change over time and characterize the behavior and motion of the vehicle. These include measurable quantities such as wheel speeds and accelerations, as well as unmeasurable states such as tire forces, tire-road characteristics, and roll angles. The parameters, on the other hand, are intrinsic properties of the vehicle that remain relatively constant during operation. These factors include the vehicle's mass, moments of inertia, center of gravity position, dimensions such as track width and wheelbase, tire properties, and suspension characteristics such as spring rates and damping coefficients.

This literature review explores the methodologies and advancements in state estimation and parameter identification for vehicle control systems. The chapter proceeds as outlined below: Section 2.1 covers various vehicle models used in the estimation schemes. Section 2.2 examines the sensor configurations and the characteristics of different sensor types. Section 2.3 reviews the existing studies on the states and parameters under estimation, including the methods for their

doi:10.6342/NTU202403171

simultaneous estimation. Section 2.4 explores the real-time estimation algorithms, such as Kalman filtering. Finally, Section 2.5 concludes the review by identifying research gaps and discussing the future prospects.

2.1 Vehicle Models

2.1.1 Kinematic Models

A kinematic vehicle model provides a mathematical representation of a machine's behavior without factoring in forces and torque. Such model comes in various forms, each tailored to specific states of concern. An example can be found in [2] , where a 3DOF estimator based on kinematics is proposed. This approach remains robust against parameter uncertainties across different road surfaces when estimating vehicle sideslip angle. However, kinematic models are prone to accumulating noise over time, leading to increased estimation errors. To address this challenge, some researchers combine kinematic-based observers with estimation using a dynamic-based model in sensor fusion schemes, as demonstrated in [3, 4].

2.1.2 Dynamic Models

In contrast to the kinematic model, dynamic models account for forces and torque exerted on both the vehicle body and tires. Estimators may employ varying degrees of freedom based on the states of interest, supported by suitable assumptions.

doi:10.6342/NTU202403171

Among these, the simplest model among these is the longitudinal motion model, which involves a single DOF. This is commonly represented by the single-track vehicle model, also referred to as the bicycle model, which could be expanded to two DOFs by incorporating lateral motion, as illustrated in Figure 2-1[5]. This model allows for a straightforward description of vehicle behavior without extensive modeling efforts.

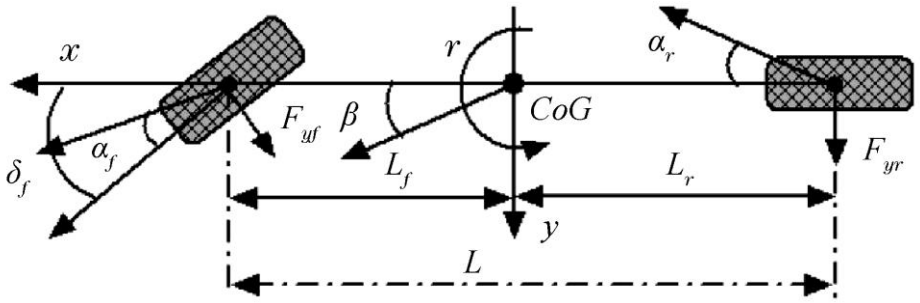

Figure 2-1 2 DOF vehicle dynamic model [5]

When considering both longitudinal and lateral motion alongside yaw rate, the 3DOF vehicle model may suffice for estimating tire-road forces seen in [6]. Incorporating additional roll leads to a 4DOF model is found in [7], suitable for methods related to roll stability control, while it ignores pitch and vertical movement. When considering individual wheel speeds in a 3DOF model, we obtain a 7DOF model where longitudinal velocity can be corrected by assuming zero slip. Similarly, adding wheel rotational speeds to a 4DOF model results in an 8DOF model, which is extensively studied in vehicle dynamics, particularly for rollover prevention.

doi:10.6342/NTU202403171

For a more comprehensive analysis, a 14 DOF model is beneficial as it describes suspension movements in detail. This model includes the vertical motion of the wheels and their speeds, alongside the six degrees of freedom of the vehicle body.

2.2 Sensor Configurations

The sensor configuration varies significantly among different vehicles based on their specific functionalities and requirements. Ideally, sensors are chosen to be as low-cost as possible due to the mass production of vehicles. For example, vehicles equipped with an Electronic Stability Program (ESP) can measure wheel velocity, steering wheel angle, longitudinal velocity, lateral acceleration and its yaw rate. This setup is the standard sensor configuration for most production vehicles. Sensors configuration should meet the requirements of ADAS, considering the specific states being estimated and the estimation method employed.

2.2.1 Steering Angle Sensors

Steering wheel angle sensors, commonly found as standard in vehicles equipped with ADAS, where the steering input can be translated into the angle of the wheels. Wheel angles are crucial for determining lateral tire forces, which are essential for calculating vehicle sideslip and yaw rate. These sensors provide critical inputs for most state estimation algorithms, enhancing vehicle control and safety.

doi:10.6342/NTU202403171

2.2.2 Wheel Speed Sensors

Wheel rotation sensors, also commonly known as wheel speed sensors, measures the rotational speed (RPM) or angular velocity (rad/s) of each wheel. It acts as a crucial component for various vehicle systems such as traction control systems (TCS) and anti-lock braking systems (ABS) to function. Usually the wheel speed sensor is used in conjunction with the steer angle sensor, acting as system inputs in model-based estimators.

2.2.3 GPS/GNSS

Global Navigation Satellite System (GNSS), commonly referred to as Global Positioning System (GPS), due to the prominence of the United States' GPS system as leading provider in GNSS technology. The use of the navigation system for vehicle dynamic state estimations measures vehicle states with high accuracy, specifically longitudinal and lateral velocities, detailed in [8]. GPS offers drift-free information, but it has downsides including high cost, slow update rates (commercially operating at 1Hz), and susceptibility to environmental influences. It is particularly affected in tunnels and underground areas where signals may be lost.

2.2.4 Inertial Measurement Unit (IMU)

An IMU is an electronic device that gives body acceleration and angular rate using its accelerometers and gyroscopes respectively. An indirect sensor approach

doi:10.6342/NTU202403171

for vehicle state estimation involves using IMUs, which perform numerical integration with data operating typically at 100Hz. However, IMUs are affected by noise and bias, leading to error accumulation over time. GNSS/GPS and IMUs are often combined for sideslip angle and yaw rate estimation, with yaw rate typically being a byproduct of sideslip angle estimation. This can be achieved either through a kinematic approach or by using these sensors as measurements in model-based approaches such as Kalman filtering. Both GPS/GNSS and IMU has its own advantages and disadvantages in state estimation, which is why they are frequently used together in sensor fusion with vehicle models.

2.3 State and Parameter Estimation

Over the years, various techniques have been suggested to address the demand of state estimation, given the diverse range of states involved. Some literature reviews have covered this topic with different approaches. [9] summarized proposed methods and techniques for estimation of various vehicle states, and [5] has conducted an expansive literature a broad spectrum of aspects including various measurements and sensor configurations, vehicle models used and estimation methodologies. Figure 2-2 illustrates how these elements of state estimation are integrated into vehicle control systems.

doi:10.6342/NTU202403171

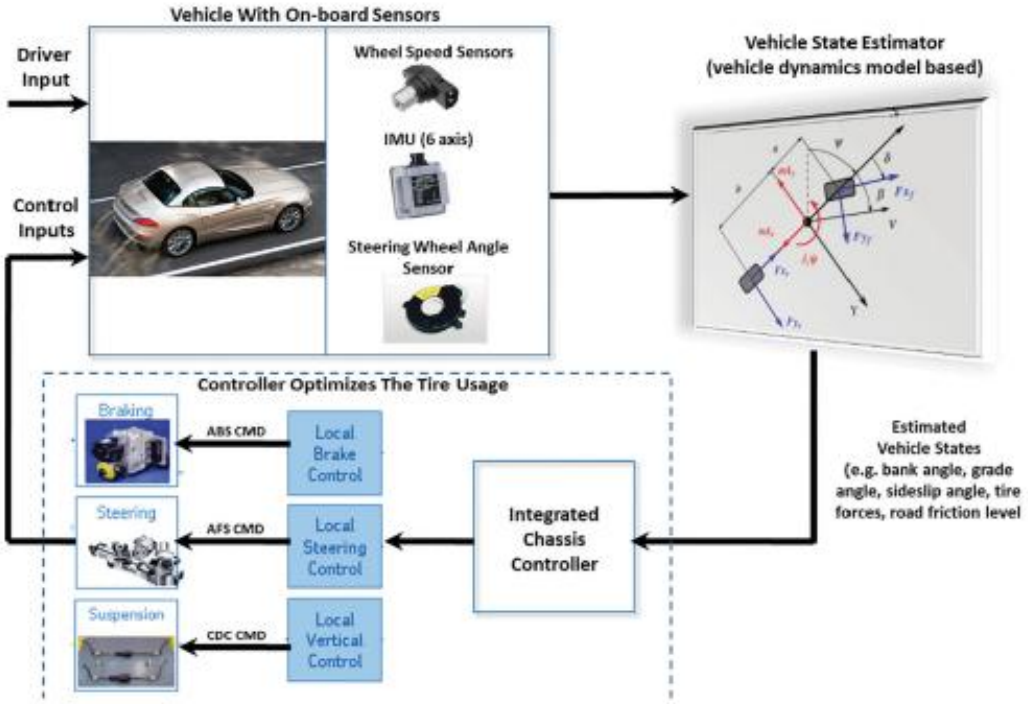

Figure 2-2 Diagram of vehicle control systems [9]

Vehicle state estimation involves calculating the current state or condition of a vehicle, including motion properties, tire forces, sideslip angles and roll, which will be discussed in this chapter. Other aspects, include road profile elevation, tire-road characteristics, road bank and road grade, as illustrated in Figure 2-3, and even "smart tires" equipped with additional sensors, represent potential advancements in vehicle control. However, these topics will not be elaborated upon in this review, as tire-road characteristics are not the main scope of this study.

doi:10.6342/NTU202403171

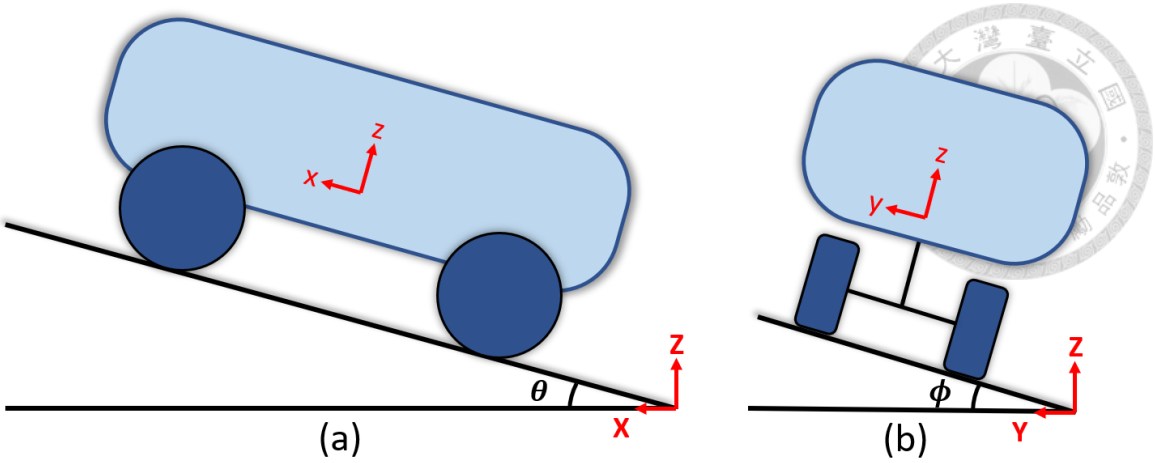

Figure 2-3 (a) Road grade angle (b) Road bank angle

2.3.1 Tire Forces

Estimating tire forces is crucial for vehicle dynamics. The process involves estimation of tire slip ratios and angles to find the lateral, longitudinal and vertical forces as well as aligning torques exerted on the tires. With knowledge of tire forces, we can determine the movement of a vehicle, this includes variables such as vehicle velocity, acceleration and angular rates. A notable example is presented in [10] where longitudinal /lateral forces of tire are estimated employing a random-walk Kalman filter, performing effectively under various conditions. [11] proposes an approach for the estimation of lateral force and sideslip angles based on an interacting multiple-model (IMM) Kalman filter, as illustrated in Figure 2-4, which switches between different models. The study also compares the performance of the interacting multiple-model Extended Kalman filter (IMM-EKF) and the interacting multiple-model Unscented Kalman filter (IMM-UKF). Other studies focus primarily on the

doi:10.6342/NTU202403171

estimation of lateral forces. Baffet et al. [12] demonstrates this in a study comparing different tire models for estimating tire slip angle, finding that a nonlinear tire model that updates cornering stiffness, gives the best results. However, this is without the evaluation of performance on low friction surfaces and banked roads.

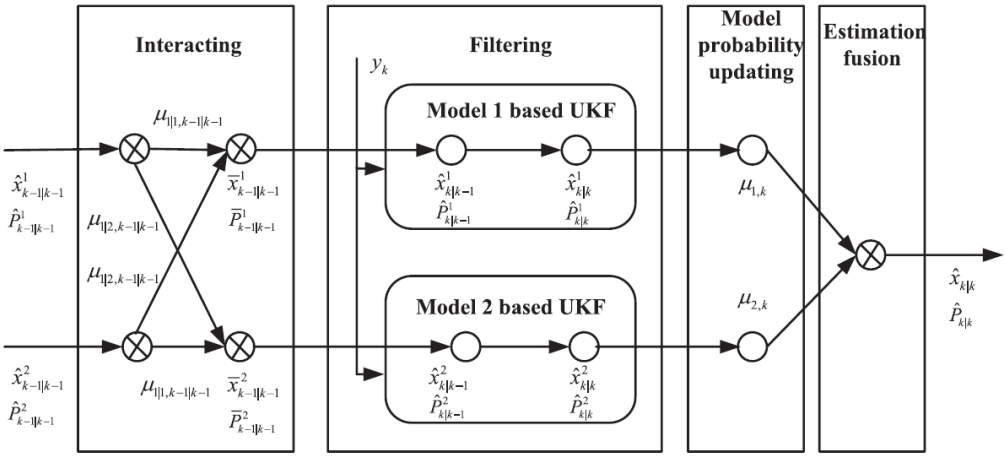

Figure 2-4 An IMM-UKF algorithm [11]

2.3.2 Sideslip Angle/ Cornering Stiffness

Lateral force of a tire increases linearly with the sideslip angle within the linear region of cornering stiffness, especially for small angles. Therefore, accurately estimating sideslip angles and cornering stiffness enhances the precision of predicting lateral tire forces. Properly managing sideslip angles optimizes grip and traction, thereby reducing the risk of losing control. Consequently, estimating sideslip angles is a common focus in vehicle dynamics research. Aoki et al. [13] achieve robust and effective sideslip angle estimation using a linear observer based on yaw rate and lateral acceleration sensors. Another study [14] compares dynamic-

doi:10.6342/NTU202403171

based and kinematic-based model approaches for sideslip angle estimation. The authors in [2] further improve sideslip angle estimation by using an Extended Kalman Filter (EKF) based on a kinematic model. This method is less affected by road friction parameter uncertainties and yields smaller estimation errors compared to previous methods. To capitalize on the benefits of dynamic model-based methods, which are less noisy, and kinematic model-based methods, which are more robust under parameter uncertainties, [15] integrates both approaches for enhanced reliability across varying tire-road conditions.

2.3.3 Velocity

The tire forces can be utilized in various ways, such as deriving the critical states of longitudinal and lateral velocity. For instance, the authors in [16] propose an algorithm to estimate longitudinal velocity by measuring wheel rotational speeds and longitudinal acceleration using a Butterworth filter to process signals. This method is feasible with data available from most commercial cars. [17] employs an Adaptive Kalman filter (AKF) for estimating lateral and longitudinal velocity, resulting in robust and accurate outcomes. Furthermore, [18] combines this method with a fuzzy logic-based longitudinal velocity estimator for use in ESC control

doi:10.6342/NTU202403171

2.3.4 Roll Analysis

The studies mentioned above use planar motion to estimate longitudinal and lateral motion alongside yaw movement. However, in some cases, estimators also account for vehicle roll angle. For instance, [19] employs a half-car vehicle model, depicted in Figure 2-5, to incorporate roll dynamics, derive the load transfer ratio, and propose a predictive load transfer ratio (LTR) that offers a predictor of rollover propensity, which benefits rollover prevention systems. Rajamani et al. [3, 4] focus on developing kinematic observers for the estimating roll angle and COG height. The studies explore two types of algorithms: one employing a sensor fusion technique and the other utilizing a nonlinear dynamic observer. The former approach integrates an additional low-frequency tilt-angle sensor with a gyroscope, while the dynamic observer relies solely on accelerometer and gyroscope data. The latter approach, which considers the vehicle's roll dynamics, offers more accurate estimations and improved performance under varying road conditions.

doi:10.6342/NTU202403171

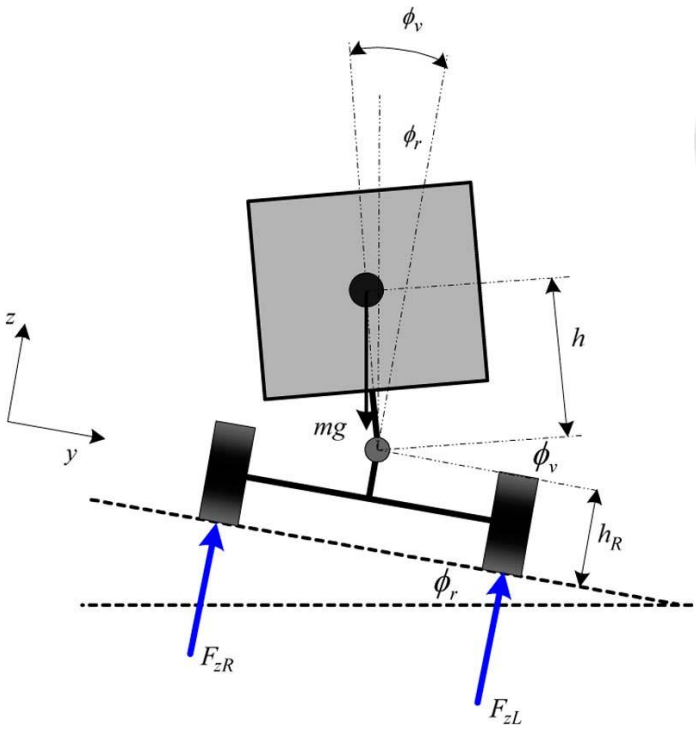

Figure 2-5 A half-car vehicle model for roll dynamics [19]

2.3.5 Vehicle Parameter Identification

Vehicle parameters, such as mass, center of gravity position and moments of inertia, can impact its safety and handling due to its influence on roll and cornering stability. Nominal values of such parameters can be obtained used commercial testbeds or static measuring methods. However, these parameters fluctuate with the vehicle's loading conditions, potentially affecting vehicle performance adversely if control systems are not adjusted accordingly. Therefore, real-time identification of inertial properties, as opposed to relying on nominal values, can optimize the effectiveness of driver assistance and stability control systems. In [20], authors develop a technique based on dynamic detection to measure COG height of a vehicle during braking, which outperforms static measurements but requires vehicles to

doi:10.6342/NTU202403171

brake on a test bench and lacks real-time capability. Authors in [21] propose a method to estimate COG height and position of a lightweight vehicle using modal analysis of free decay response, achieving low relative errors in their results. Solmaz et al.[22] implement real-time estimation of COG height and tire stiffness using linear vehicle models, highlighting the critical role of COG height in rollover prevention systems. Zarringhalam et al.[23] investigate and compare four methods for estimating vehicle inertial parameters: Gradient method, the Recursive least squares method (RLS), Kalman Filtering (KF), and Extended Kalman Filtering (EKF). Their study demonstrates that the EKF is particularly effective for estimating mass, moments of inertia, and COG location of a vehicle.

2.3.6 State and Parameter Estimation

Previous studies have explored how parameter identification affects the accuracy of state estimates, revealing insights into their interdependence. Certain studies focus on simultaneous simulation of state and parameter estimation, employing two distinct filtering techniques for states and parameters. This approach is often referred to as Dual Kalman filtering.

The Dual EKF originated from the concept a weighted EKF developed by Wan and Nelson [24], which involves running two EKFs in parallel. Wenzel et al. [7] were the first to apply this concept to nonlinear vehicle dynamics systems. Hong et al. [25,

doi:10.6342/NTU202403171

26] advanced this approach by incorporating the roll degree of freedom and transitioning from the EKF to the UKF. This dual filtering technique, separately estimating states and parameters is also observed in [27], where a DEKF-based estimator was introduced for estimating the tire cornering stiffness. Additionally, [28] employs an AKF for state estimation, while an EKF is utilized for estimating COG position. The dual filtering approach is also seen in [29], where the proposed algorithm estimates states and parameters for heavy articulated vehicles.

2.4 Estimation Methodology

Building upon the previously provided states, sensor configurations, and vehicle modeling, this section explores real-time estimation methods.

2.4.1 Kalman Filtering

This category includes the Kalman Filter (KF), Recursive Least Squares (RLS) and more advanced configurations such as the Extended Kalman Filter (EKF), Unscented Kalman Filter (UKF), and alternative methods such as Adaptive Kalman Filter (AKF) and particle filters. The RLS method can be considered as a special case of the KF[30].

Research [31] demonstrates the use of an EKF technique as a model-based vehicle state estimator. Comparative studies, such as those in [7] and [23], evaluate

doi:10.6342/NTU202403171

RLS, RKF and EKF in estimating a vehicle parameters, with findings pointing to the EKF as the most reliable method for real-time estimation.

The UKF, introduced by Julier and Uhlmann [32] and elaborated by Wan and van der Merwe [33], approximates the system around multiple points [24] and can achieve better results than an EKF in highly nonlinear systems. For instance, [34] incorporates the UKF with a 3DOF vehicle model that includes yaw, longitudinal and lateral motion generating estimates of yaw rate and vehicle sideslip that closely match the actual states. Hong et al. [26] compare the EKF and UKF by implementing both in a Dual Kalman Filter scheme for a 4DOF nonlinear vehicle parameter identification algorithm, concluding that the UKF performs better, albeit with higher computational demands. Both EKF and UKF exhibit similar convergence characteristics and yield similar results.

Additionally, [28] proposes an estimation method utilizing an optimization-based AKF to filter noisy states, coupled with an EKF for parameter estimation. The AKF adjusts the process noise covariance in real-time through an optimization process aimed at minimizing bias and fluctuation in the state estimate [35].

In conclusion, Kalman filtering and its advanced variants are integral to real-time vehicle state and parameter estimation. The EKF stands out for its reliability in dynamic, model-based estimations, while the UKF offers superior performance in

doi:10.6342/NTU202403171

terms of accuracy. The AKF further enhances estimation by dynamically adjusting to minimize errors.

2.4.2 Other Methods

Observer-based methods are commonly used for estimating vehicle states. Two kinematics-based linear observers (LO) are used for estimating vehicle roll and pitch angles utilizing an inertial measurement unit in [36]. Nonlinear observers (NLO) have been extensively researched, and a comparative study [37] indicates that NLOs are less complex and sometimes perform better than EKFs for estimating vehicle velocity, although they are less stable under varying parameter conditions. Besides NLOs, sliding mode observers (SMO) are also employed. In [38] , the authors compare LO, NLO, SMO, and EKF for estimating vehicle sideslip. The results indicate that all methods yield similar results at low speeds, but at high acceleration, the observers require more accurate assumptions for effective performance.

Machine learning methods are also utilized in vehicle state estimation, with artificial neural networks (ANN) being a prominent example. ANNs are algorithms inspired by the structure and function of animal brains. In [39] , ANN is used to estimate vehicle sideslips, achieving satisfactory results in most maneuvers. However, understanding the underlying mechanisms of this method is challenging, and different surface conditions may be inadequately addressed, necessitating further

doi:10.6342/NTU202403171

investigation. Similar to ANN, fuzzy logic is applied to sideslip estimation in [40]. However, fuzzy logic has drawbacks as it relies heavily on specified parameters and fuzzy rules, making it challenging for engineering applications due to the vast variability in driving conditions.

Additionally, optimization-based methods like moving horizon estimation (MHE) are applied in vehicle state estimation. For example, in [41] , MHE is employed to estimate lateral acceleration, yaw rate and vehicle sideslip. Estimation results achieved for yaw rates by MHE surpasses that of the UKF. However, MHE requires significant computational effort, and reducing this burden while estimating additional states remains an area for further research.

2.5 Conclusion of Literature Review

In summary, the literature review highlights the advanced developments of state estimation, facilitated by affordable equipment, and utilization of sophisticated methodologies. However, there remains a gap in simultaneous estimation of both states and parameters, with vehicle mass being the primary parameter identified thus far. Further research into additional inertial information could significantly enhance the efficacy of ADAS in stability control systems. Additionally, the focus on light-weight and passenger vehicles underscores the need for further development in load-

doi:10.6342/NTU202403171

carrying vehicles and trailers, which are not only essential for transportation but also more susceptible to accidents. Moving forward, addressing these gaps will be vital for enhancing safety and efficiency across diverse vehicle types.

doi:10.6342/NTU202403171

Chapter 3 Dual Extended Kalman Filter

3.1 Dynamics Systems

3.1.1 Linear Dynamic Systems

A general state-space representation of a linear dynamic system is expressed as follows:

$$\dot{x}(t) = A(t)x(t) + B(t)u(t) \quad (3.1)$$

$$y(t) = C(t)x(t) + D(t)u(t) \quad (3.2)$$

In this context, x is the state vector, u is input (control) vector, y is the output (measurement) vector; the system is described by matrices: A (state/system matrix), B (input matrix), C (output matrix) and D (feedforward matrix).

In its general form, these matrices are typically time-variant, except in cases where the system operates under linear time-invariant (LTI) conditions, where they remain constant over time. The system can be continuous, where time t serves as the time-variable, or discrete, where the time-variable is indexed by k.

3.1.2 Nonlinear Dynamic Systems

For both linear and nonlinear systems, a broader form of state-space representation is expressed as:

$$\dot{x}(t) = f\big(t, x(t), u(t)\big) \quad (3.3)$$

$$y(t) = h\big(t, x(t), u(t)\big) \quad (3.4)$$

doi:10.6342/NTU202403171

where *f* represents the state function, while *h* denotes the measurement or output function. If the functions are linear combinations of states and inputs, the equations can subsequently be formulated using matrices as described earlier. The input u(t) can be disregarded if the system has no inputs.

3.1.3 Discretization of Continuous Systems

While most state-space representations of physical systems are defined using differential equations and derived in a continuous form, it is necessary to convert these into a discrete form for certain applications. This conversion process, known as discretization, involves approximating the continuous-time model to be represented in the discrete domain. This allows for the effective implementation of the Kalman filter and other similar algorithms, which operate as discrete algorithms.

Building on the continuous-time state-space representations (3.1) and (3.2) previously formulated, we can reformulate the equations describing relations between the state vector, input and output matrices to be represented in the discrete domain. This is done by assuming zero-order hold for the inputs, meaning that the input signal remains constant within each sampling interval of duration T. The derivation of this reformulated relationship is detailed in [42]. The discrete-time representation of a linear system becomes:

doi:10.6342/NTU202403171

$$x_k = e^{AT}x_{k-1} + (\int_0^T e^{AT}dt)Bu_{k-1} \quad (3.5)$$

$$y_k = C_k x_k + D_k u_k \quad (3.6)$$

Exact calculation of the state-space model may become challenging due to complexity of calculations involving large matrices and integral operations. To overcome this, a common method is to use the approximation $e^{AT} \approx I + AT$ to derive a discrete-time model with the assumption of a small sampling time T. This method is known as the Euler or forward Euler method. The solution is then approximated as:

$$x_k = (I + AT)x_{k-1} + TBu_{k-1} \quad (3.7)$$

$$y_k = C_k x_k + D_k u_k \quad (3.8)$$

3.1.4 Linearization of Dynamic Systems

To analyze a nonlinear system, we can approximate its behavior by linearizing it around an operating point (x_0). This linearization allows us to leverage the established methods of discretization for linear systems, mentioned earlier. A standard approach is to perform a Taylor series expansion around point (x_0) and disregard higher-order terms. In the algorithm presented in this thesis, the linearization is put into practice as the Extended Kalman Filter by recursively updating the point at which the system in linearized. The iterative process is detailed in Chapter 3.2.3.

doi:10.6342/NTU202403171

3.2 Kalman Filter

3.2.1 History of the Kalman Filter

In 1960, Rudolf Emil Kálmán first published his first paper on linear filtering [43], which laid the foundation for what would become known as the Kalman filter. This approach employs a series of mathematical formulas to recursively estimate the states of dynamic systems. Widely applied in signal processing, control systems, and navigation for autonomous systems [44]. The Kalman filter also serves as a powerful solution for observing unmeasurable states or fusing sensor data, even in scenarios where system characteristics are uncertain.

3.2.2 Concept of the Kalman Filter

Assuming the discrete state-space representation of a linear dynamic system is modeled as follows:

$$\mathrm{x_k} = Ax_{k-1} + Bu_{k-1} + w_{k-1} \quad (3.9)$$

$$\mathrm{y_k} = Hx_k + v_k \quad (3.10)$$

$\mathrm{w_k}$ represents the system's process noise, and v_k represents the measurement noise at each timestep. Both are assumed to follow independent Gaussian distributions with the following properties:

doi:10.6342/NTU202403171

$$p(w) \sim N(0, Q) \quad (3.11)$$

$$p(v) \sim N(0, R) \quad (3.12)$$

where probability distributions of variable w and v have a mean vector of 0, follows Gaussian distribution and has process noise covariance Q and measurement covariance R, respectively.

To derive equations for the filter, the first step is to derive the *a posteriori* state estimate $\hat{x}_k$. This estimate is a linear combination of the a priori state estimate $\hat{x}_k^-$ and the residual. The residual is the difference between measurement y_k and the predicted measurement $H\hat{x}_k^-$, mathematically expressed as $(y_k - H\hat{x}_k^-)$.

$$\hat{x}_k = \hat{x}_k^- + (y_k - H\hat{x}_k^-) \quad (3.13)$$

where K_k is the Kalman gain, formulated to minimize estimation errors, defined as:

$$K_k = \frac{\Phi_k^- H^T}{H\Phi_k^- H^T + R} = \Phi_k^- H^T (H\Phi_k^- H^T + R)^{-1} \quad (3.14)$$

The Kalman gain is defined in such a way that as measurement error covariance R approaches zero, K gives more weight to the residual, thereby directing the a posteriori state estimate towards the measurement.

$$\lim_{R \to 0} K_k = \lim_{R \to 0} \frac{\Phi_k^- H^T}{H\Phi_k^- H^T + R} = H^{-1} \quad (3.15)$$

$$\hat{x}_k = \hat{x}_k^- + K_k(y_k - H\hat{x}_k^-) = \hat{x}_k^- + H^{-1}(y_k - H\hat{x}_k^-) = y_k \quad (3.16)$$

doi:10.6342/NTU202403171

As the state covariance Φ_k^- of each step approaches zero, K reduces weights on the residual, directing the *a posteriori* state estimate to approach the *a priori* state estimate.

$$\lim_{\Phi_k^- \to 0} K_k = \lim_{\Phi_k^- \to 0} \frac{\Phi_k^- H^T}{H\Phi_k^- H^T + R} = 0 \quad (3.17)$$

$$\hat{x}_{\mathrm{k}} = \hat{x}_{\mathrm{k}}^- + \mathrm{K}(\mathrm{y}_{\mathrm{k}} - H\hat{x}_{\mathrm{k}}^-) = \hat{x}_{\mathrm{k}}^- + 0(\mathrm{y}_{\mathrm{k}} - H\hat{x}_{\mathrm{k}}^-) = \hat{x}_{\mathrm{k}}^- \quad (3.18)$$

As measurement error covariance R goes towards zero, reliance on actual measurement increases, while confidence in the prediction decreases. Conversely, as *a priori* estimate error covariance Φ_k^- approaches zero, trust in the sensor measurement decreases, and confidence in the prediction increases.

3.2.3 Equations of a Kalman Filter

The Kalman Filter is a recursive estimation algorithm designed for linear dynamic systems. It uses noisy measurements to generate an optimal estimate of the system's state vector. The filter operates in two steps: the time update, or prediction step, and the measurement update, or correction step, as illustrated in Figure 3-1 below.

doi:10.6342/NTU202403171

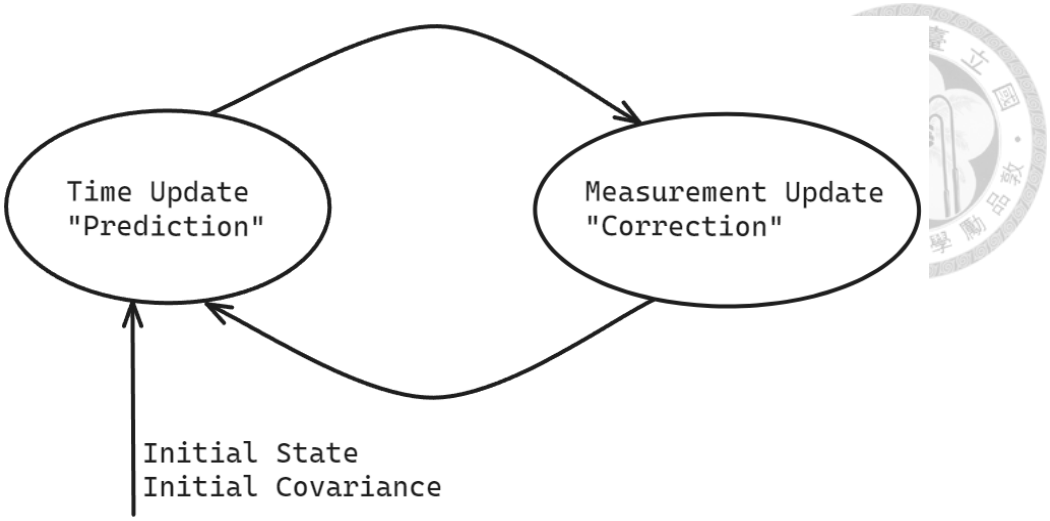

Figure 3-1 The Kalman Filter cycle

Time Update/ Prediction Step

This step predicts the current state of the system according to the previous state and the system dynamics model. It predicts both the state vector and the covariance matrix from the previous time step.

$$\hat{x}_k^- = A\hat{x}_{k-1}^- + Bu_{k-1} \quad (3.19)$$

$$\Phi_k^- = A\Phi_{k-1}A^T + Q \quad (3.20)$$

Measurement Update/ Correction Step

First, the filter computes the Kalman gain. This value determines the weight assigned between the current measurement and the predicted state estimate. Using this gain, the filter corrects the predicted state estimate by incorporating the difference between the actual measurement and the predicted measurement. Finally, the filter updates the error covariance matrix, which reflects the uncertainty in the state estimate.

doi:10.6342/NTU202403171

$$K_k = \Phi_k^- H^T (H\Phi_k^- H^T + R)^{-1} \quad (3.21)$$

$$\hat{x}_k = \hat{x}_k^- + K_k(y_k - H\hat{x}_k^-) \quad (3.22)$$

$$\Phi_k = (I - K_k H)\Phi_k^- \quad (3.23)$$

These steps are repeated recursively for each time step, providing an optimal estimate of the system state by combining predictions from the system model with measurements from sensors, while accounting for process and measurement noise.

3.2.4 Extended Kalman Filter

The Extended Kalman Filter is "extended" from a linear Kalman Filter to tackle non-linear systems, while the KF is restricted to linear systems. Here's how the EKF achieves this:

(1) *Linearization*: The nonlinear system equations are linearized around a specific operating point. This process creates a local linear approximation of the system's behavior at that point.

(2) *Recursive Update*: Unlike the KF, which uses fixed system matrices, the EKF continuously updates these linearized matrices as the states change. It uses the current state estimate as the new operating point for the next linearization, applying the Kalman Filter at each recursive step.

doi:10.6342/NTU202403171

The EKF is essential for the estimating non-measurable states of vehicle systems. As most vehicle models are non-linear, such as the one proposed for this thesis in Chapter 4.1.2. Despite its capabilities, the EKF is suboptimal and may not be suitable for highly nonlinear systems. In such cases, alternatives such as the UKF and particle filters can offer more effective solutions.

Consider a discrete-time representation of a non-linear dynamic system:

$$x_k = f(x_{k-1}, u_{k-1}, w_{k-1}) \quad (3.24)$$

$$y_k = h(x_k, v_k) \quad (3.25)$$

Prediction equations of an EKF:

$$\hat{x}_k^- = f(\hat{x}_k^-, u_{k-1}) \quad (3.26)$$

$$\Phi_k^- = J_k \Phi_{k-1} J_k^T + R \quad (3.27)$$

Correction equations of an EKF:

$$K_k = \Phi_k^- H_k^T (H_k \Phi_k^- H_k^T + \sigma)^{-1} \quad (3.28)$$

$$\hat{x}_k = \hat{x}_k^- + K_k(y_k - h(\hat{x}_k^-)) \quad (3.29)$$

$$\Phi_k = (I - K_k H_k)\Phi_k^- \quad (3.30)$$

The matrix J is defined as the Jacobian matrix of the dynamic equations evaluated at the *a priori* state estimate:

$$J_k = \frac{\partial f(x)}{\partial x}|_{x=\hat{x}_k^-} \quad (3.31)$$

doi:10.6342/NTU202403171

The matrix H is defined as the Jacobian matrix of the measurement equations evaluated at the *a priori* state estimate:

$$H_k = \frac{\partial h(x)}{\partial x}|_{x=\hat{x}_k^-} \quad (3.32)$$

3.3 Dual Extended Kalman Filter

The concept of a Dual EKF was first proposed by Nelson and Stear in [45], enabling simultaneous estimation of both states and parameters of a system. This approach showcases its versatility for various applications, including:

(1) *Estimation*: The filter is employed to reduce noise and achieve a clean state.

(2) *Prediction*: It utilizes knowledge of the system to forecast future states.

(3) *Identification*: It focuses on uncovering the underlying parameters of the system.

The DEKF is derived from weight estimation of a system where parameters of the system can be determined using clean data. However, when only noisy data is available, a two-step process is employed to estimate the weights, as elaborated by Wan and Nelson in [24]. First, an initial EKF estimates the states using preliminary weights. Then, a second EKF is refines the weight estimation, enhancing the overall accuracy and robustness of the system's state and parameter estimation, as illustrated in Figure 3-2.

doi:10.6342/NTU202403171

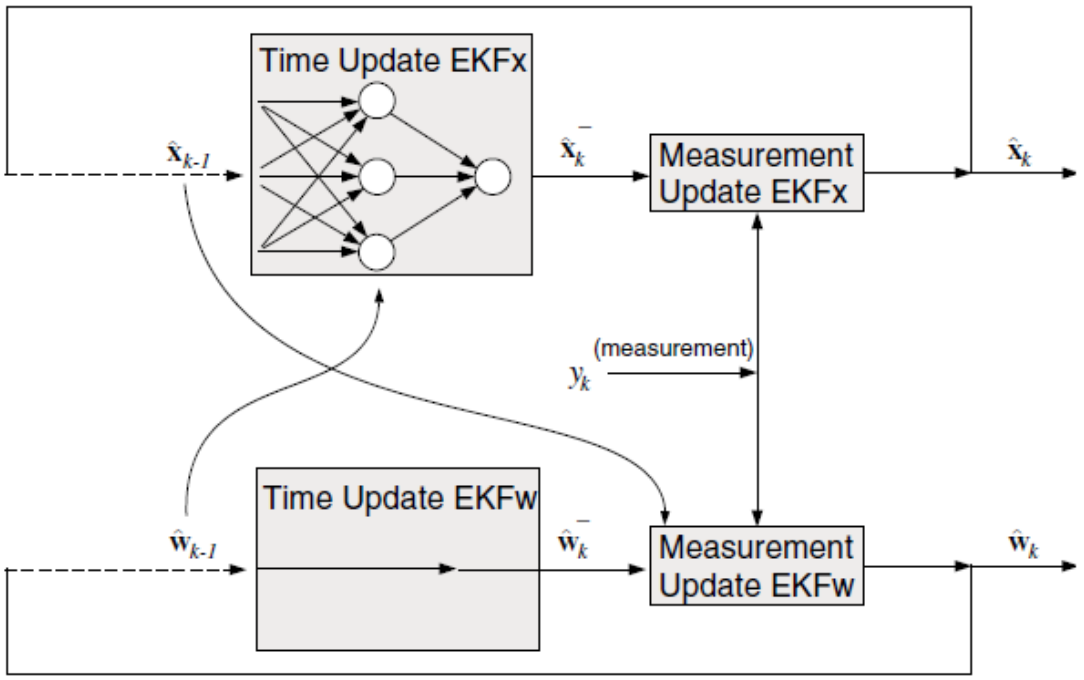

Figure 3-2 Scheme of a DEKF [24]

For a weighted non-linear dynamic system as below

$$\mathrm{x_k} = \mathrm{f}\left(\mathrm{x}_{s,k-1}, x_{p,k-1}, u_{k-1}, w_{k-1}\right) \quad (3.33)$$

$$\mathrm{y_k} = h(x_{s,k}, \mathrm{x}_{p,k}, v_k) \quad (3.34)$$

The equations of a DEKF can be formulated as with the following four steps:

Parameter prediction

$$\hat{x}_{\mathrm{p}}^-(t) = \hat{x}_{\mathrm{p}}^-(t-1) \quad (3.35)$$

$$\Phi_{\mathrm{k}}^-(t) = \Phi_{\mathrm{k}}^-(t-1) + \mathrm{R_p} \quad (3.36)$$

State prediction

$$\hat{x}_{\mathrm{s}}^-(t) = f\left(\hat{x}_s^-(t-1), \hat{x}_p^-(t), u(t)\right) \quad (3.37)$$

$$\Phi_{\mathrm{s}}^-(t) = J_s(t)\Phi_s^-(t-1)J_s^T(\mathrm{t}) + \mathrm{R_s} \quad (3.38)$$

doi:10.6342/NTU202403171

State correction

$$\mathrm{K_s}(t) = \Phi_s^-(t)H_s^T(H_s\Phi_s^-H_s^T + \sigma_s)^{-1} \quad (3.39)$$

$$\hat{x}_s(t) = \hat{x}_s^-(t) + K_s(t)(y(t) - H_s\hat{x}_s^-(t)) \quad (3.40)$$

$$\Phi_s(t) = (I - K_k(t)H_s)\Phi_s^-(t) \quad (3.41)$$

Parameter correction

$$\mathrm{K}_p(t) = \Phi_p^-(t)H_p^T\left(H_p\Phi_p^-(t)H_p^T + \sigma_p\right)^{-1} \quad (3.42)$$

$$\hat{x}_p(t) = \hat{x}_p^-(t) + K_p(t)(y(t) - H_s\hat{x}_s^-(t)) \quad (3.43)$$

$$\Phi_p(t) = \left(I - K_p(t)H_p\right)\Phi_p^-(t) \quad (3.44)$$

Symbols σ_s and σ_p denote the measurement covariance of state correction and parameter correction respectively. These measurement covariances are determined according to the sensor specifications, which are detailed in Section 5.3.2 for the proposed algorithm.

The matrix J is defined as the Jacobian matrix of the dynamic equations evaluated at the *a priori* estimate:

$$J_s = \frac{\partial f(x)}{\partial x}|_{x=\hat{x}_k^-} = \begin{bmatrix} \frac{\partial f_1}{\partial x_1} & \cdots & \frac{\partial f_1}{\partial x_m} \\ \vdots & & \vdots \\ \frac{\partial f_m}{\partial x_1} & \cdots & \frac{\partial f_m}{\partial x_m} \end{bmatrix} \quad (3.45)$$

doi:10.6342/NTU202403171

The matrix H_s is defined as the Jacobian matrix of the measurement equations evaluated at the *a priori* estimate:

$$H_s = \frac{\partial h(x)}{\partial x}|_{x=\hat{x}_k^-} \quad (3.46)$$

H_p may be acquired using the following relationship:

$$H_p = H_s \frac{\partial f(x_s, x_p)}{\partial x_p} \quad (3.47)$$

R_p is the initial covariance matrix of the parameter estimator, which is more sensitive to covariance matrix settings. Each diagonal value in R_p is set to approximately 1% of the actual parameter values. R_s is the initial covariance matrix of the state estimator and can be set as an identity matrix with constant values as diagonal elements.

doi:10.6342/NTU202403171

Chapter 4 Vehicle model

4.1 4-DOF Vehicle Model

4.1.1 Vehicle Coordinates:

In this paper vehicle dynamics are described using z-down vehicle coordinates specified in SAE J670 [46], as shown in Figure 4-1. This coordinate system refers to a coordinate system where the z-axis points downwards from the vehicle's COG towards the ground, essential for analyzing the motion and behavior of vehicles.

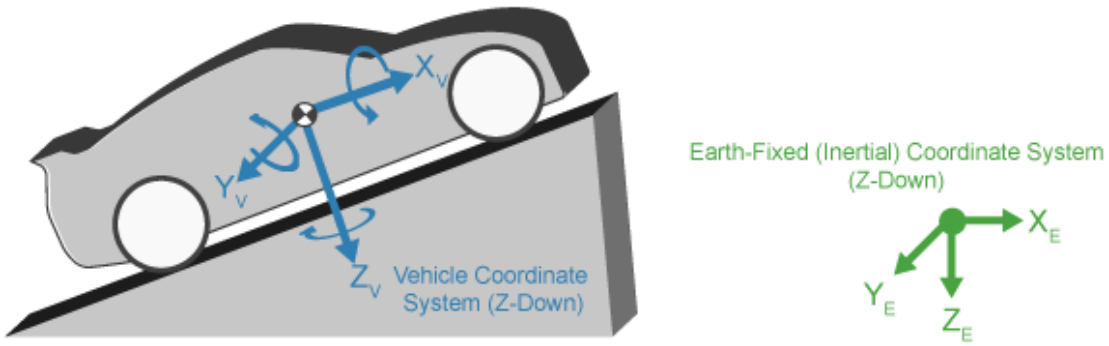

Figure 4-1 Vehicle coordinates [47]

The six degrees of freedom in vehicle dynamics include longitudinal, lateral, and vertical motions, as well as roll, yaw and pitch. Longitudinal motion refers to forward and backward movements along the vehicle's axis, while lateral motion denotes side-to-side movements, and vertical motion involves upward and downward movements. Additionally, rotations around each axis encompass roll (around the longitudinal axis), pitch (around the lateral axis), and yaw (around the vertical axis).

doi:10.6342/NTU202403171

4.1.2 Vehicle Dynamic Equations

The estimation algorithm uses a four degree-of-freedom model which include the vehicle's longitudinal motion, lateral motion, roll, and yaw. The symbols x, y, ϕ, ψ represent each dimension respectively. The definition of coordinates and parameters of this vehicle model is depicted in Figure 4-2 below.

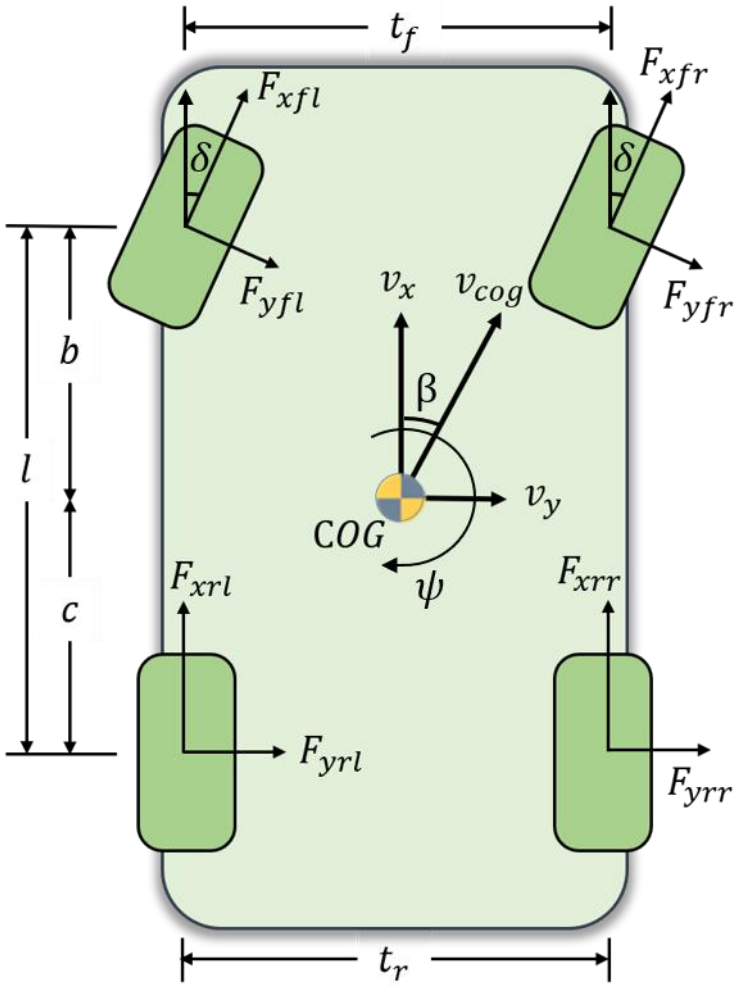

Figure 4-2 Coordinates and parameters of vehicle model

The primary states, derived from continuous-time representations of the system's equations, include longitudinal velocity v_x, lateral velocity v_y, yaw rate $\dot{\psi}$, roll angle ϕ and roll rate $\dot{\phi}$. the rates of velocity change, and the yaw and roll motions around

doi:10.6342/NTU202403171

the center of gravity. In addition to these measurable states, there are non-measurable or derived states, including longitudinal acceleration a_x, lateral acceleration a_y, sensor-based lateral acceleration $a_{y,sensor}$, slip angles s_{ij}, tire slip angles α_{ij}, vertical tire forces F_{zij}, vehicle sideslip angle β, and lateral load transfer ratio (LTR). These derived states provide further insight into vehicle dynamics and are crucial for comprehensive vehicle state estimation. These states are detailed by the differential equations presented in this chapter.

The parameters that are estimated in the proposed algorithm include vehicle mass m, yaw moment of inertia I_z, center of gravity longitudinal position b, roll moment of inertia I_x and center of gravity height h_s. Fixed values for additional vehicle parameters are provided in Appendix B.

Table 4-1 Estimated states and parameters

Primary states	$v_x, v_y, \dot{\psi}, \phi, \dot{\phi}$
Derived states	$a_x, a_y, a_{y,sensor}, s_{ij}, \alpha_{ij}, F_{zij}, \beta, LTR$
Estimated parameters	m, I_z, b, I_x, h_s

Longitudinal and lateral motion

According to Newton's law of motion and geometric relationships found in [48], longitudinal and lateral acceleration can be found as:

doi:10.6342/NTU202403171

$$a_x = \frac{1}{m}(F_{xfl}cos\delta - F_{yfl}sin\delta + F_{xfr}cos\delta - F_{yfr}sin\delta + F_{xrl} + F_{xrr}) \quad (4.1)$$

$$a_y = \frac{1}{m}\left(F_{yfl}cos\delta + F_{xfl}sin\delta + F_{yfr}cos\delta - F_{xfr}sin\delta + F_{yrl} + F_{yrr}\right) \quad (4.2)$$

where δ is the tire steer angle.

The rate of change of longitudinal and lateral velocities are given by:

$$\dot{v_x} = a_x + v_y\dot{\psi} \quad (4.3)$$

$$\dot{v_y} = a_y - v_x\dot{\psi} \quad (4.4)$$

Yaw motion

Lateral tire forces are the primary contributors to yaw moments in a vehicle. When a vehicle turns, the tires generate lateral forces due to the slip angles. The difference in lateral force between the front and rear tires generates a moment about the z-axis, leading the vehicle to rotate around its vertical axis.

$$\ddot{\psi} = \frac{\Gamma}{I_z} \quad (4.5)$$

$$\begin{aligned}\Gamma = {} & \frac{t_f}{2}\left(F_{xfl}cos\delta - F_{yfl}sin\delta\right) - \frac{t_f}{2}\left(F_{xfr}cos\delta - F_{yfr}sin\delta\right) \\ & + \frac{t_r}{2}F_{xrl} - \frac{t_r}{2}F_{xrr} + b\left(F_{yfl}cos\delta + F_{xfl}sin\delta\right) \\ & + b\left(F_{yfr}cos\delta + F_{xfr}sin\delta\right) - cF_{yrl} - cF_{yrr} \\ & + M_{zfl} + M_{zfr} + M_{zrl} + M_{zrr}\end{aligned} \quad (4.6)$$

Roll motion

doi:10.6342/NTU202403171

To construct the system state-space function with roll angle ϕ as a primary state in the algorithm, its time derivative $\dot{\phi}$ is expressed as the continuous-time equation below, relating the value at the current time step to the previous one. This formulation enables the calculation of the vehicle's roll angle through integration of the roll rate:

$$\dot{\phi}_{\mathrm{k}} = \dot{\phi}_{k-1} \tag{4.7}$$

The time derivative of the roll rate is described as a relationship between the roll moment of inertia and total roll moment of the unsprung mass.

$$\ddot{\phi} = \frac{1}{I_x}(m_s h_s a_y + \phi(m_s g h_s - \kappa_\phi) - \dot{\phi}\beta_\phi) \tag{4.8}$$

κ_ϕ and β_ϕ are roll stiffness and roll damping coefficients, respectively.

Lateral slip

Lateral slip occurs when the direction in which a wheel is pointing differs from the actual motion of the tire. This discrepancy is also known as the slip angle, and is vital for determining lateral forces and self-aligning moments exerted by a tire, as well as understanding the cornering behavior of and vehicle. The slip angles for all four tires are calculated as follows:

$$\alpha_{fl} = \delta - arctan(\frac{v_y + b\dot{\psi}}{v_x + \frac{t_f}{2}\dot{\psi}}) \tag{4.9}$$

$$\alpha_{fr} = \delta - arctan(\frac{v_y + b\dot{\psi}}{v_x - \frac{t_f}{2}\dot{\psi}}) \tag{4.10}$$

doi:10.6342/NTU202403171

$$\alpha_{rl} = arctan(\frac{-v_y + c\dot{\psi}}{v_x + \frac{t_r}{2}\dot{\psi}}) \quad (4.11)$$

$$\alpha_{rr} = arctan(\frac{-v_y + c\dot{\psi}}{v_x - \frac{t_r}{2}\dot{\psi}}) \quad (4.12)$$

Vehicle sideslip angle

The vehicle sideslip angle, also known as the body slip angle, refers to the angle between the x-axis and the actual velocity direction of a vehicle. Sideslip angle is a crucial parameter in vehicle dynamics as it directly influences the vehicle's handling during maneuvers, especially during cornering. Sideslip angle is calculated as follows:

$$\beta = arctan(\frac{v_y}{v_x}) \quad (4.13)$$

Longitudinal slip

Longitudinal slip occurs when a torque is applied to a wheel axle, creating a contact force exerted between the road surface and the tires. Resulting in difference between rotational motion of the wheel and actual vehicle velocity relative to the road. Typically expressed as a percentage, longitudinal slip here is defined by ratio as follows:

$$s_{ij} = \frac{\omega_{ij} r}{v_{ij}} - 1 \quad (4.14)$$

doi:10.6342/NTU202403171

In static vehicles, where there is no relative motion between the tires and road surface, tire slip is undefined.

Tire velocity

The velocity of each tire is derived in accordance with vehicle velocity while considering the yaw rate and vehicle sideslip. Here v_{ij} represents the velocity of each tire:

$$v_{fl} = v_{CoG} + \dot{\psi}(\frac{t_f}{2} - b\beta) \quad (4.15)$$

$$v_{fr} = v_{CoG} + \dot{\psi}(-\frac{t_f}{2} - b\beta) \quad (4.16)$$

$$v_{rl} = v_{CoG} + \dot{\psi}(\frac{t_f}{2} + c\beta) \quad (4.17)$$

$$v_{rr} = v_{CoG} + \dot{\psi}(-\frac{t_f}{2} + c\beta) \quad (4.18)$$

Vertical tire forces

Vertical forces, also referred to as normal forces, significantly affect the grip and traction of a tire, thereby being directly linked to the stability of a vehicle. During acceleration and braking, weight transfers from front to back and back to front, respectively. Additionally, weight transfers from side to side during cornering. By using longitudinal and lateral acceleration data and considering the overall load distribution, the tire vertical forces are defined respectively as follows:

$$F_{zfl} = \left(\frac{1}{2}mg + ma_y\frac{h_s}{t_f}\right)\frac{c}{l} - \frac{1}{2}(ma_x\frac{h_s}{l}) \quad (4.19)$$

$$F_{zfr} = \left(\frac{1}{2}mg - ma_y\frac{h_s}{t_f}\right)\frac{c}{l} - \frac{1}{2}(ma_x\frac{h_s}{l}) \quad (4.20)$$

doi:10.6342/NTU202403171

$$F_{zrl} = \left(\frac{1}{2}mg + ma_y\frac{h_s}{t_r}\right)\frac{b}{l} + \frac{1}{2}(ma_x\frac{h_s}{l}) \quad (4.21)$$

$$F_{zrr} = \left(\frac{1}{2}mg - ma_y\frac{h_s}{t_r}\right)\frac{b}{l} + \frac{1}{2}(ma_x\frac{h_s}{l}) \quad (4.22)$$

Load transfer ratio

Load transfer refers to the change of vertical forces experienced by each individual wheel of a vehicle. The Load Transfer Ratio (LTR) is a dimensionless metric that indicates the degree of this change. The LTR ranges from 1, indicating that all weight is on the left wheels, to -1, indicating that all weight is on the right wheels. Ideally, the LTR should be zero with the vehicle in a neutral position. The load transfer ratio serves as an important indicator and is one of several variables applied in assessing the rollover propensity in stability control systems.

$$LTR = \frac{F_{z,l} - F_{z,r}}{F_{z,l} + F_{z,r}} \quad (4.23)$$

4.2 Tire Model

4.2.1 Tire Coordinate System

The tire coordinate system is pivotal in vehicle dynamics as it provides a frame of reference for understanding tire behavior and interaction with the road surface. This coordinate system usually aligns with the wheel's rotational axis, where the x-axis directs forward along the direction of travel, the y-axis extends sideways across

doi:10.6342/NTU202403171

the tire's width, and the z-axis is perpendicular to the ground. In this system, the tire contact patch serves as the origin, where forces and moments acting on the tire are measured and analyzed, as demonstrated in Figure 4-3 below. The tire's behavior is influenced by various factors such as camber angles, slip angles and vertical loads, which affect its performance in terms of traction, cornering stiffness, and rolling resistance.

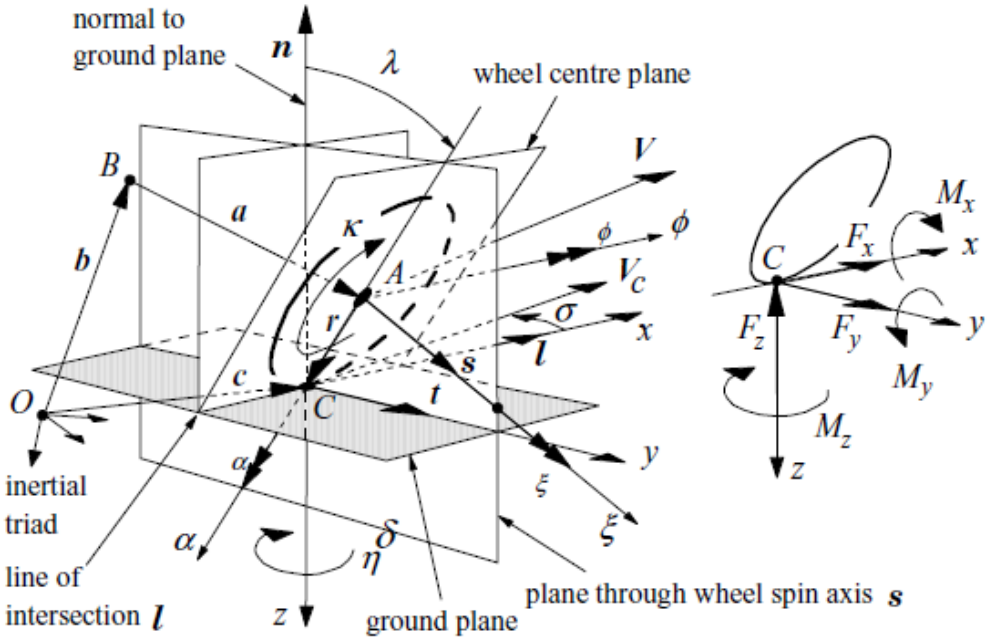

Figure 4-3 Motion and forces/moments of a wheel [49]

Tire forces typically include longitudinal forces, lateral forces, and vertical forces. Longitudinal forces, also known as traction or braking forces, are responsible for propelling or decelerating the vehicle. Lateral forces, in contrast, act perpendicular to the direction of travel and are generated during cornering maneuvers, providing the necessary grip to maintain control and stability. Vertical forces, or tire

doi:10.6342/NTU202403171

load, represent the weight of the vehicle and any additional loads exerted on the tire, influencing its contact pressure with the road surface.

In addition to forces, moments are also significant in tire dynamics. Moments include moments around the longitudinal, lateral and vertical axis. Roll moments occur when tire torque tilts or leans it relative to the vehicle's longitudinal axis, impacting cornering stability. Pitch moments arise from torques that cause the tire to rotate around its lateral axis, influencing the vehicle's response to acceleration and braking forces. Yaw moments result from torques that cause the tire to rotate around its vertical axis, impacting the vehicle's directional stability and steering control.

4.2.2 The Magic Formula Tire Model

The Magic Formula tire model, developed by Pajecka [49], is used to determine steady-state tire forces and moments for vehicle dynamics. The semi-empirical model has become a cornerstone in vehicle dynamics simulations and racing games due to their versatility and broad applicability across various tire constructions and operating conditions. Other tire models, such as TMeasy and the Fiala tire model, operate similarly. However, according to [7], the Magic Formula provides superior results, which is why this modeling method is chosen for the simulation.

The general form of the Magic Formula, as proposed by Pacejka, involves a set of fitting constants, B, C, D, and E, relating slip parameter x to resulting forces or

doi:10.6342/NTU202403171

moments, offering a flexible framework that has served as the foundation for numerous derivative models.

The magic formula tire model is described in [49] as a general formula as below:

$$y(x) = Dsin\big(C\arctan\big(B - E(B - \arctan B)\big)\big) \quad (4.24)$$

$$Y(X) = y(x) + S_v \quad (4.25)$$

$$x = X + S_h \quad (4.26)$$

The variables are defined as follows: *Y* represents the output variable, which could be longitudinal force (F_x), lateral force (F_y), or aligning torque (M_z). *X* denotes the input variable, such as tangent of slip angle (α) or slip ratio (κ). B stands for the stiffness factor, while C represents the shape factor. D denotes the peak value, and E is the curvature factor. S_H and S_V indicate horizontal and vertical shifts, respectively, in the model equations.

The name "Magic Formula" reflects the model's ability to fit a wide range of empirical data through a series of equations characterized by multiple coefficients. These coefficients encapsulate the complex relationship between tire behavior and parameters such as vertical load, camber angle, and slip angle.

doi:10.6342/NTU202403171

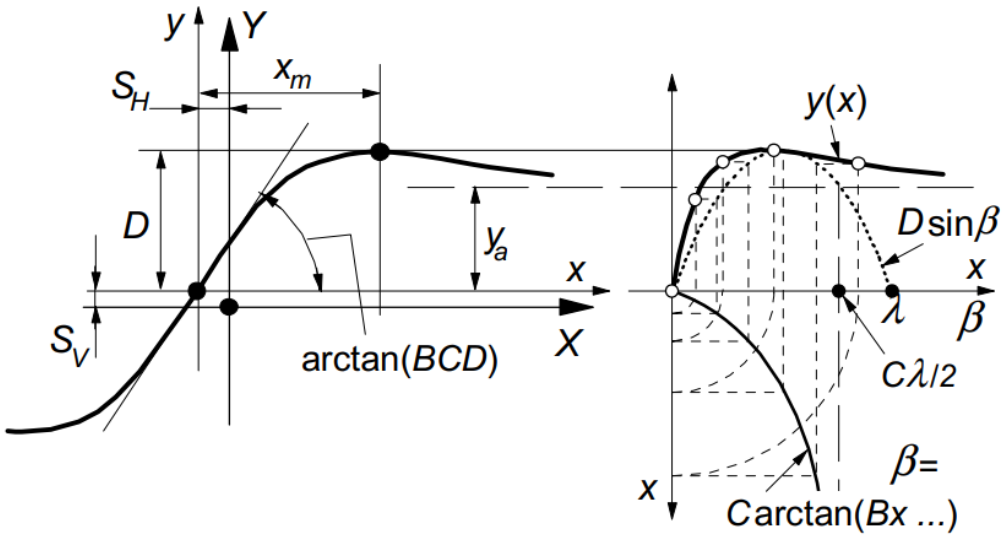

Figure 4-4 The Magic Formula tire model [49]

4.2.3 Full Set of Tire Modeling Equations

In the full set of equations for tire forces and torque in this chapter, df_z denotes normalized change in vertical load:

$$df_z = (F_z - F_{z0})/F_{z0} \quad (4.27)$$

where F_{z0} represents the nominal vertical load of a tire. User scaling factors λ are introduced to adjust the formula, with default values set to 1 when not specified. The coefficients for defining the forces and torque of the test tires—provided by dSPACE (dry tire set)—can be found in Appendix B.

doi:10.6342/NTU202403171

Pure longitudinal slip

The calculation for pure longitudinal slip is as follows:

$$\mathrm{F_x} = D_x \sin\big(C_x \arctan\big(B_x\kappa_x - E_x(B_x\kappa_x - \arctan(B_x\kappa_x))\big)\big) \quad (4.28)$$

$$+ S_{Vx}$$

$$\kappa_x = \kappa + S_{Hx} \quad (4.29)$$

$$\mathrm{C_x} = p_{Cx1}\lambda_{Cx} \quad (4.30)$$

$$\mathrm{D_x} = \mu_x F_z \quad (4.31)$$

$$\mu_x = (p_{Dx1} + p_{Dx2}df_z)\lambda_{\mu x} \quad (4.32)$$

$$\mathrm{E_x} = (p_{Ex1} + p_{Ex2}df_z + p_{Ex3}df_z^2) * \{1 - p_{Ex3}sgn(\kappa_x)\} * \lambda_{Ex} \quad (4.33)$$

$$\mathrm{K_{x\kappa}} = F_z * (p_{\mathrm{K}x1} + p_{\mathrm{K}x2} * df_z) * exp(p_{Kx3} * df_z) * \lambda_{\mathrm{K}z\kappa}(\quad (4.34)$$

$$= B_xC_xD_x = \frac{\partial F_{x0}}{\partial \kappa_x}\ at\ \kappa_x = 0)$$

$$\mathrm{B_x} = \mathrm{K}_x/(C_xD_x) \quad (4.35)$$

$$\mathrm{S_{Hx}} = (p_{Hx1} + p_{Hx2}df_z)\lambda_{Hz} \quad (4.36)$$

$$\mathrm{S_{Vx}} = F_z * (p_{Vx1} + p_{Vx2}df_z)\lambda_{Vx}\lambda_{\mu x} \quad (4.37)$$

doi:10.6342/NTU202403171

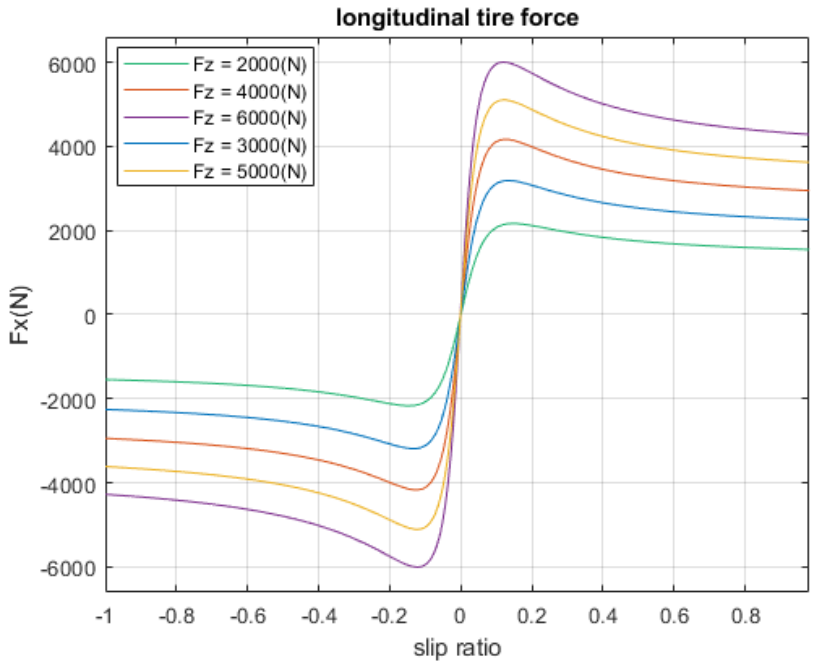

Figure 4-5 Tire longitudinal force curves

Pure lateral slip

The calculation for pure longitudinal slip is as follows:

$$\mathrm{F_y} = D_y \sin\left(C_y \arctan\left(B_y\alpha_y - E_y\left(B_y\alpha_y - \arctan\left(B_y\alpha_y\right)\right)\right)\right) + S_{Vy} \quad (4.38)$$

$$\alpha_\mathrm{y} = \alpha + S_{Hy} \quad (4.39)$$

$$\mathrm{C_y} = p_{Cy1}\lambda_{Cy} \quad (4.40)$$

$$\mathrm{D_y} = \mu_y F_z \quad (4.41)$$

$$\mu_\mathrm{y} = \left(\mathrm{p_{Dy1}} + \mathrm{p_{Dy2}} df_z\right)\lambda_{\mu\mathrm{y}} \quad (4.42)$$

$$\mathrm{E_y} = \left(p_{Ey1} + p_{Ey2} df_z\right) * \left\{1 - \left(p_{Ey3} + p_{Ey4}\gamma^*\right) sgn\left(\alpha_y\right)\right\} * \lambda_{Ey} \quad (4.43)$$

doi:10.6342/NTU202403171

$$\mathrm{K_{y\alpha}} = p_{\mathrm{Ky1}} F_{z0} \sin[2\arctan\{F_z/(p_{\mathrm{Ky2}} F_{z0})\}] * \left(1 - p_{\mathrm{Ky3}} \gamma^{*2}\right) \lambda_{\mathrm{Ky}} (\quad (4.44)$$

$$= B_y C_y D_y = \frac{\partial F_{y0}}{\partial \kappa_y} \; at \; \kappa_x = 0)$$

$$\mathrm{B_y} = \mathrm{K}_y/(C_y D_y) \quad (4.45)$$

$$\mathrm{S_{Hx}} = \left(p_{Hy1} + p_{Hy2} df_z\right) \lambda_{Hy} + p_{Hy3} \gamma^* * \lambda_{\mu y} \quad (4.46)$$

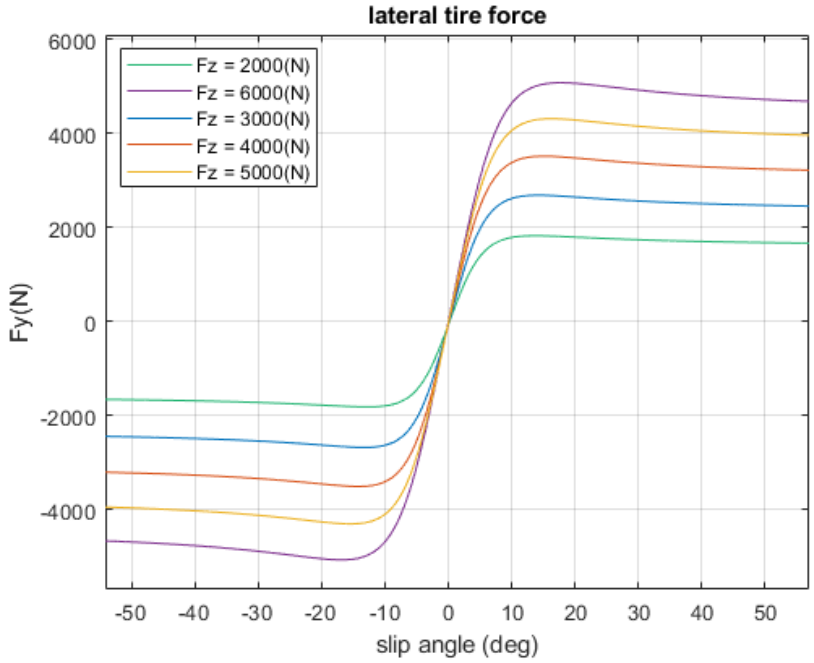

Figure 4-6 Tire lateral force curves

Aligning torque

The self-aligning torque is calculated as follows:

$$\mathrm{M_z} = M'_{z0} + M_{zr0} \quad (4.47)$$

$$\mathrm{M'_{z0}} = -t_0 * F_{y0} \quad (4.48)$$

$$\mathrm{t_0} = t(\alpha_t) = \mathrm{D_t} \cos[C_t arctan\{B_t \alpha_t \quad (4.49)$$

$$- E_t(B_t \alpha_t - \arctan(B_t \alpha_t))\}] * \cos(\alpha)$$

doi:10.6342/NTU202403171

$$\alpha_t = \alpha^* = S_{Ht} \quad (4.50)$$

$$S_{Ht} = q_{Hz1} + q_{Hz2}df_x = (q_{Hz3} + q_{Hz4}df_z)\gamma^* \quad (4.51)$$

$$M_{zr0} = M_{zr}(\alpha_r) = D_r \cos[\arctan(B_r\alpha_r)] \quad (4.52)$$

$$\alpha_r = \alpha^* + S_{Hf}(= \alpha_f) \quad (4.53)$$

$$S_{Hf} = S_{Hy} = \frac{S_{Vy}}{K'_{ya}} \quad (4.54)$$

$$K'_{ya} = K_{ya} + \epsilon_k \quad (4.55)$$

$$B_t = (q_{Bz1} + q_{Bz2}df_z + q_{bz3}df_z^2) * (1 + q_{Bz5}|\gamma^*| + q_{Bz6}\gamma^{*2}) \quad (4.56)$$

$$* \lambda_{Kya}/\lambda^*_{\mu y}$$

$$C_t = q_{Cz1} \quad (4.57)$$

$$D_t = F_z * \left(\frac{R_0}{F'_{z0}}\right) * (q_{dz1} + q_{Dz2}df_z^2) * \lambda_t * signV_{cx}(1 \quad (4.58)$$

$$+ q_{Dz3}|\gamma^*| + q_{Dz4}\gamma^{*2})$$

$$E_t = (q_{Bz1} + q_{Bz2}df_z + q_{bz3}df_z^2) \quad (4.59)$$

$$* \left\{1 + \frac{(q_{Ez4} + q_{Ez5}\gamma^*)2}{\pi}\arctan(B_tC_t\alpha_t)\right\}$$

$$B_r = q_{Bz0} * \frac{\lambda_{Ky}}{\lambda^*_{\mu y}} + q_{Bz10}B_yC_y \quad (4.60)$$

$$D_r = F_zR_0\{(q_{Dz6} + q_{Dz7}df_z) * \lambda_{Mr} + (q_{dDz8} + q_{Dz9df_z}) \quad (4.61)$$

$$* \gamma^*\lambda_{Kzy}\} * \cos(\alpha) * \lambda^*_{\mu y}$$

doi:10.6342/NTU202403171

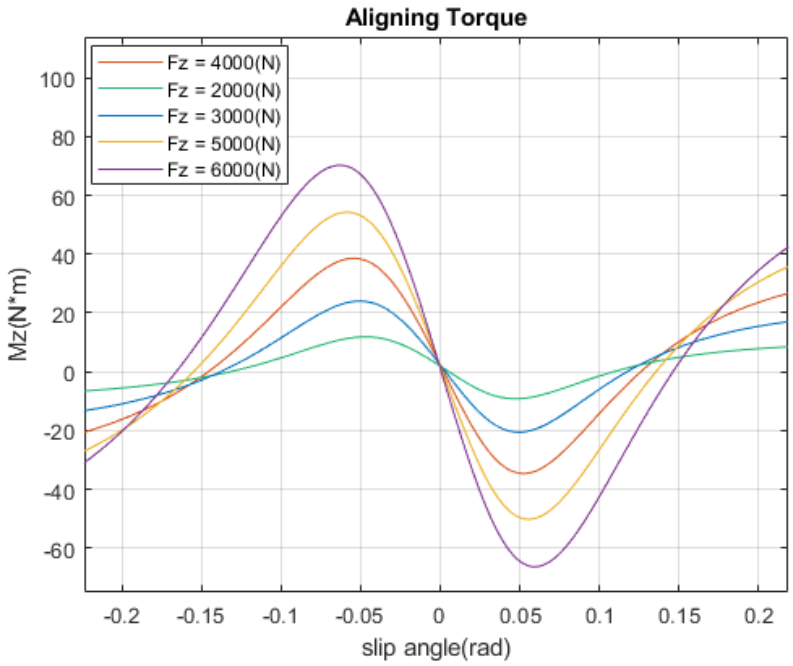

Figure 4-7 Tire self-aligning torque curves

4.3 Estimator Settings

4.3.1 Weighting Covariance

An exponential weighting methodology is implemented for the process covariance R_p. This is represented by the equation:

$$R_p(k+1) = \lambda R_p(k) \qquad (4.62)$$

where λ is the decay factor. By applying this exponential weighting, the algorithm gives more weight to recent measurements, improving the accuracy of state estimates over time. The parameter update process eventually converges, making the initial choice of R_p less significant if the weighting/decay factor λ is appropriately tuned.

doi:10.6342/NTU202403171

4.3.2 Relationship Between Parameters

The parallel-axis theorem can be used to determine the moment of inertia when modifying a vehicle's weight distribution. According to this theorem, the moment of inertia around a parallel axis z' is equal to the sum of the moment of inertia about the centroidal axis I_{cm} and the product of the object's mass and the square of the distance of these two axes.

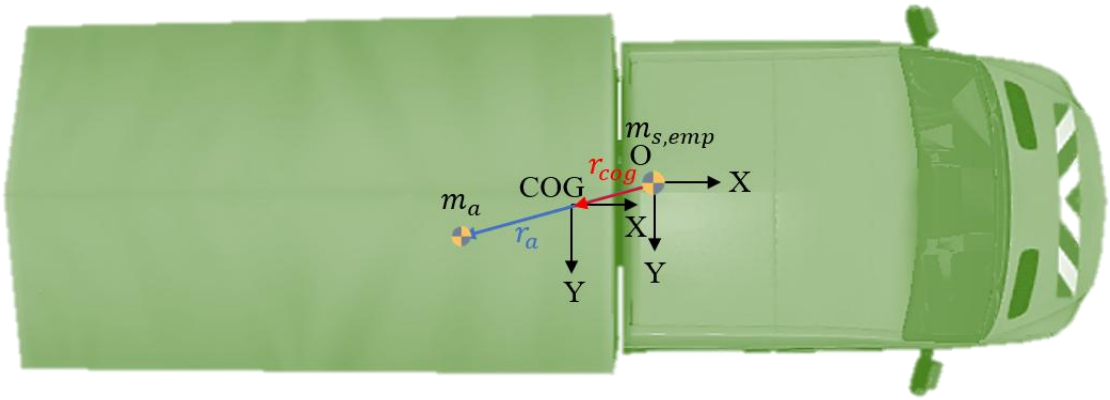

Figure 4-8 Top view of vehicle [50]

Assume an additional load m_a is added to the vehicle, with the distance between this additional mass and the origin being r_a. According to the parallel axis theorem, the moment of inertia with respect to the original coordinate frame O (I_z^O) is expressed as:

$$I_z^O = I_{z,emp} + m_a r_a^2 \quad (4.63)$$

Furthermore, the yaw moment of inertia I_z can be expressed relative to the new COG as follows:

doi:10.6342/NTU202403171

$$I_z^O = I_z + m_s r_{cog}^2 \quad (4.64)$$

where $I_{z,emp}$ denotes the yaw moment of inertia of the empty vehicle, m_s denotes the vehicle total weight with an additional load, r_{cog} is the distance from the COG to the origin.

Given the following relationships:

$$m_s = m_{s,emp} + m_a \quad (4.65)$$

$$m_s \mathrm{r_{COG}} = m_{s,emp} * 0 + m_a r_a \quad (4.66)$$

We can derive the relationship:

$$\mathrm{r_a} = \frac{m_s}{m_a} \mathrm{r_{cog}} \quad (4.67)$$

Substituting this into the previous equations (4.63) and (4.64), we get:

$$I_z = I_{z,emp} + m_a r_a^2 \ - m_s r_{COG}^2 = I_{z,emp} - \frac{m_s}{m_a}(m_s - m_a) r_{cog}^2 \quad (4.68)$$

r_{cog} is split into x and y components:

$$r_{cog}^2 = \left(l_{w,emp} - l_w\right)^2 + \left(b_{emp} - b\right)^2 \quad (4.69)$$

Assuming the COG position in the transverse direction is not estimated, we let $l_{w,emp} = l_w$. Therefore, the moment of inertia can be derived using the additional mass and its longitudinal position.:

$$I_z = I_{z,emp} - \frac{m_s}{m_a}(m_s - m_a)\left(b_{emp} - b\right)^2 \quad (4.70)$$

doi:10.6342/NTU202403171

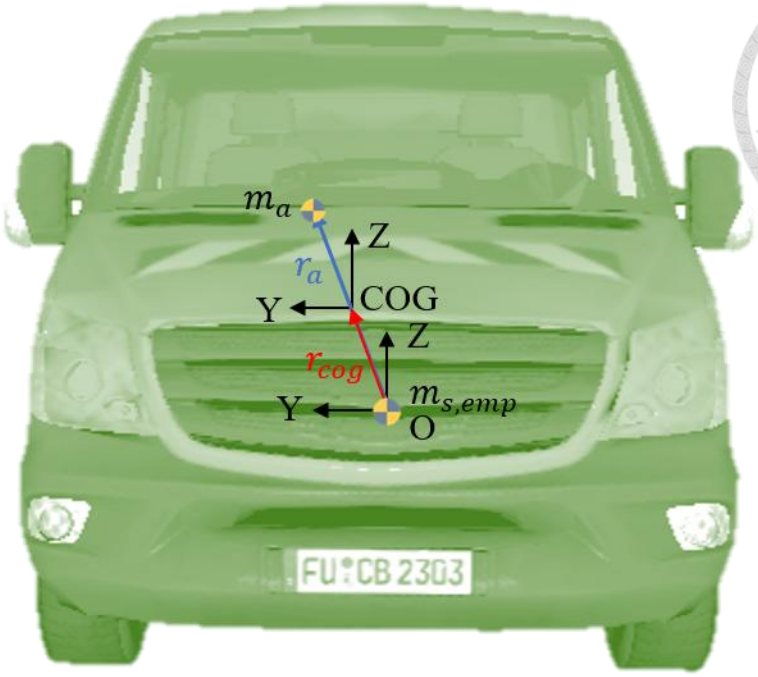

Figure 4-9 Front view of vehicle [50]

Similarly, we can derive the relationship between parameters to obtain moments of inertia on the YZ plane:

$$I_x = I_{x,emp} - \frac{m_s}{m_a}(m_s - m_a)\left(h_{s,emp} - h_s\right)^2 \quad (4.71)$$

where $I_{x,emp}$ denotes roll moment of inertia about x-axis of the empty vehicle, $h_{s,emp}$ represents the COG height of the empty vehicle, and h_s is the COG height of a loaded vehicle.

A limitation of this method is that it assumes the additional mass to be a point mass which simplifies calculations but does not account for the actual distribution of the mass.

doi:10.6342/NTU202403171

Chapter 5 Simulation

5.1 Simulation Structure

In the experiment to validate the estimation algorithm, a virtual vehicle is used instead of an actual test vehicle. Using a simulation tool is compelling due to its cost-effectiveness compared to traditional physical vehicle testing.

The estimation algorithm proposed is implemented using MATLAB/Simulink, chosen for its real-time execution capabilities and compatibility with the virtual vehicle platform. The Simulink block diagram demonstrates the operation of the algorithm as detailed in Appendix A. The algorithm operates in parallel to the multibody virtual vehicle developed by dSPACE.

The process begins by taking inputs from the vehicle system, which is then fed into the algorithm to conduct a *a priori* prediction steps of the Dual Extended Kalman Filter. Subsequently, sensor measurements from the virtual test vehicle are utilized to update the critical states and parameters, resulting to an *a posteriori* corrected value. The process in depicted in Figure 5-1.

doi:10.6342/NTU202403171

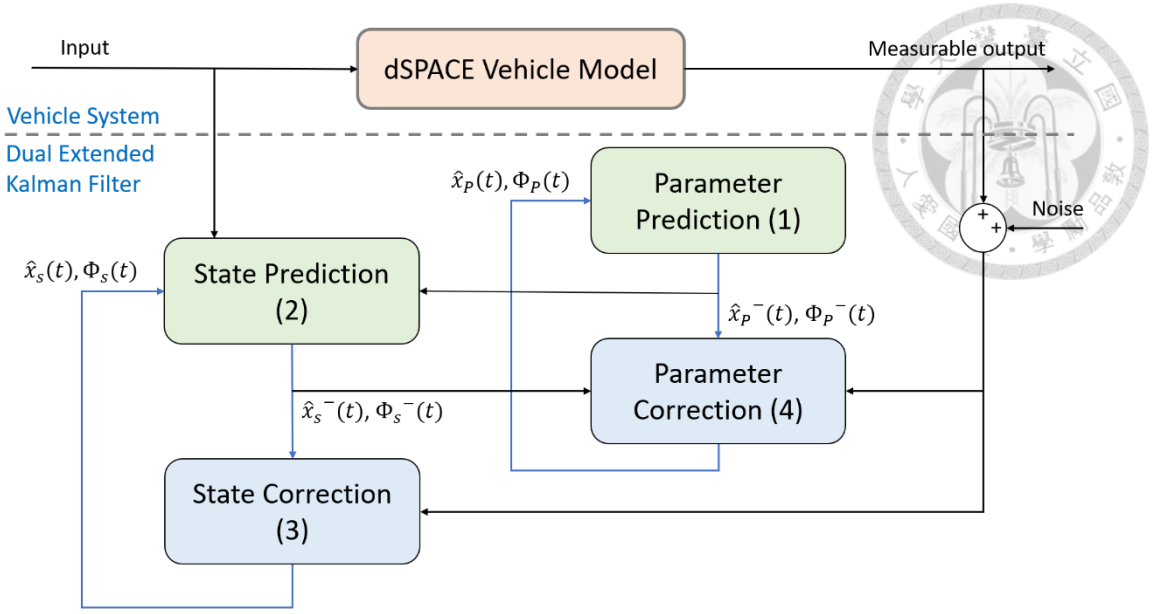

Figure 5-1 Scheme of simulation

An advantage of this structure, as introduced in [7] , is the capability for partial switch-off. This feature allows parameter prediction and correction to be turned off after the values converge, reducing the computational power required, as demonstrated in Figure 5-2 below.

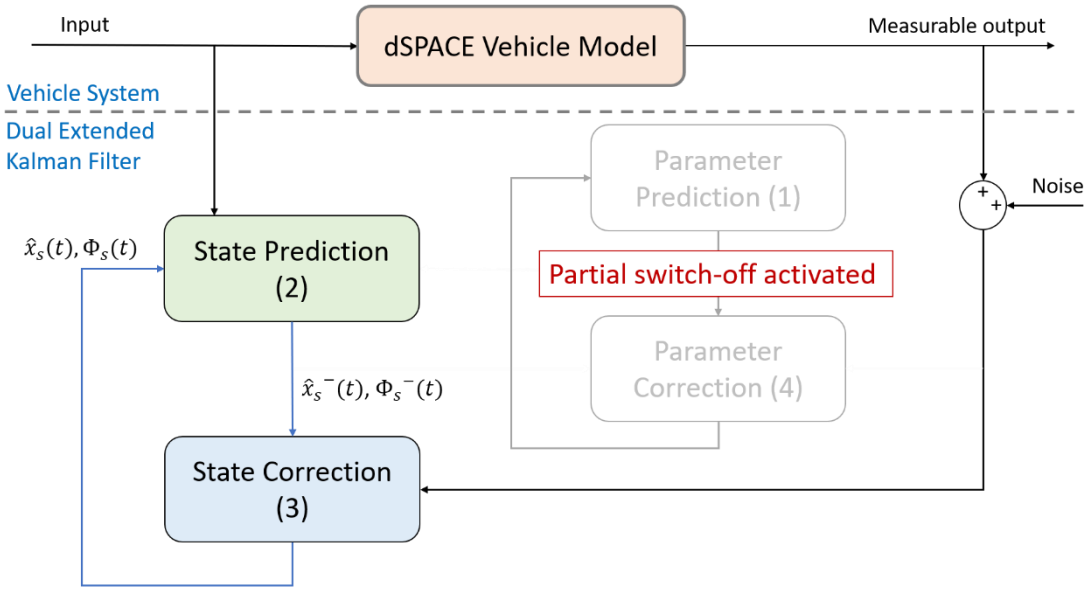

Figure 5-2 Scheme of simulation with partial switch-off

doi:10.6342/NTU202403171

5.2 Simulation Environment

The dSPACE ASM Vehicle Dynamics toolset [50] provides a controlled and replicable testing environment, enabling systematic exploration of state estimation algorithms under diverse conditions. Vehicle configurations and environmental conditions can be easily implemented without additional physical resources. Conducting tests in a virtual realm also mitigates safety concerns. The flexibility of dSPACE tools, including customizable maneuver configurations, enhances efficiency by enabling experimentation without temporal or geographical constraints, allowing iterative testing and rapid algorithm refinement.

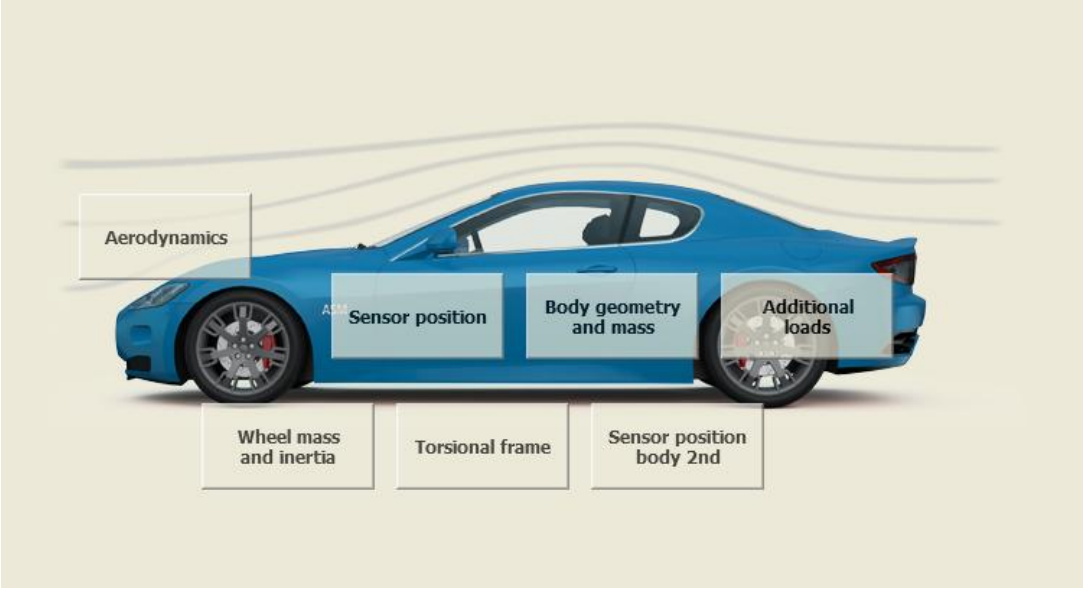

Figure 5-3 User interface of dSPACE software [50]

doi:10.6342/NTU202403171

Additionally, having full knowledge of actual vehicle parameters without the interference of sensor noise and environmental factors is a key advantage. Being cost-effective, accessible, and scalable, the virtual vehicle serves as a valuable surrogate platform for real-world experimentation.

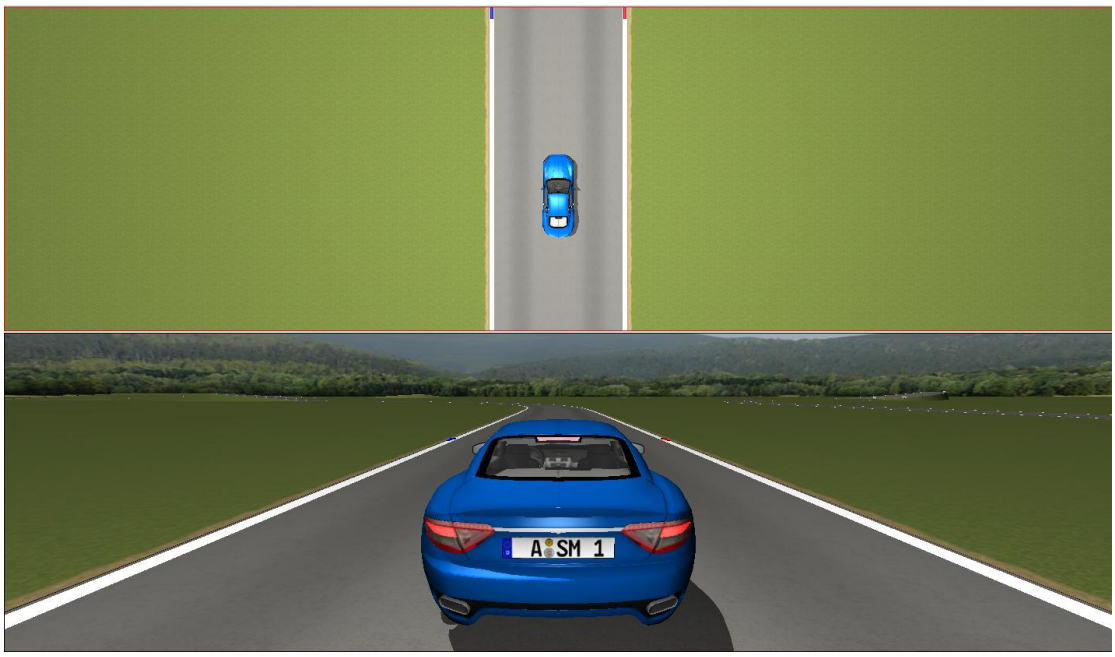

Figure 5-4 Virtual test ground visualization of dSPACE [50]

5.3 Simulation Settings

5.3.1 Vehicle Loads

Inertial parameters are configured by specifying the mass and inertial properties of the empty vehicle and additional loads in dSPACE, as illustrated in Figure 5-5. The inertial parameters of each test case are calculated using the vehicle parameters and additional loads specified in Appendix B.

doi:10.6342/NTU202403171

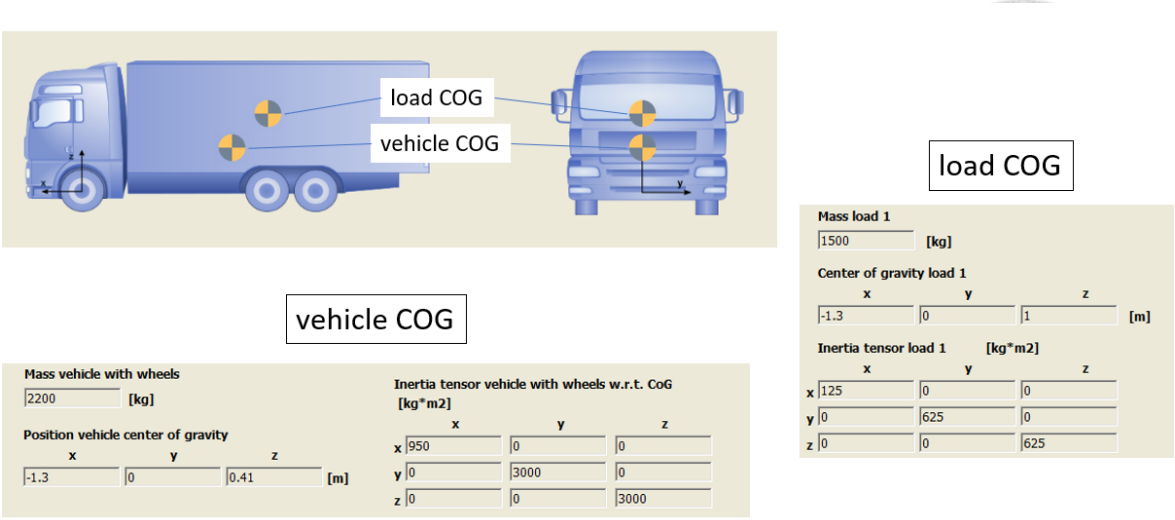

Figure 5-5 Parameter configuration in dSPACE software [50]

In this simulation, three loading conditions are tested, ranging from a fully loaded vehicle to an empty one, to cover a broad spectrum of loading scenarios. The parameters of each loading condition are specified in Table 5-1 below.

Table 5-1 Vehicle inertial parameters with additional weights

	Unladen	**Load1**	**Load2**
Mass m(kg)	2200	3700	2700
Moment of inertia about z-axis $I_z(\mathrm{kg} * \mathrm{m}^2)$	3000	3700	3216.3
CoG longitudinal position b(m)	1.3	1.38	1.34
Moment of inertia about x-axis $I_x(\mathrm{kg} * \mathrm{m}^2)$	950	1385	1171
CoG height h_s(m)	0.41	0.649	0.52

doi:10.6342/NTU202403171

5.3.2 Sensor Configuration

Inertial Measurement Unit

Standard sensors in modern cars equipped with ESP and ABS sensors usually have yaw rate, longitudinal velocity and lateral acceleration sensors. However, the proposed method considers roll dynamics, and these conventional sensors are insufficient. To fully utilize the 4-degree-of-freedom model described in 4.1.2, the algorithm requires accelerometers and gyroscopes, commonly found in the form of an Inertial Measurement Unit. The measurements required in this simulation are yaw and roll rates alongside longitudinal and lateral acceleration of the vehicle COG. This data acquisition is essential for accurate state estimation and for identifying inertial parameters of the vehicle.

In this simulation, the Inertial Measurement Unit (IMU) is modeled using Simulink's three-axis inertial measurement unit block, shown in Figure 5-6. The noise power specifications are set to match those of a standard MEMS-type IMU, as detailed in [51].

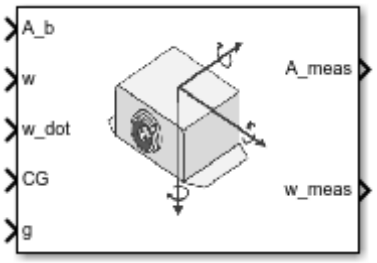

Figure 5-6 Simulink three-axis inertial measurement unit block [47]

doi:10.6342/NTU202403171

In the proposed estimators, both for state and parameters, the same measurements are utilized, resulting in equal measurement covariances: $\sigma_s = \sigma_p$, denoted as σ. Assuming all sensors are independent, σ is set to a diagonal matrix where each of the diagonal elements represent the variance of each sensor.

$$\sigma = \begin{bmatrix} \sigma_{\dot{\psi}}^2 & 0 & 0 & 0 \\ 0 & \sigma_{a_y}^2 & 0 & 0 \\ 0 & 0 & \sigma_{\dot{\phi}}^2 & 0 \\ 0 & 0 & 0 & \sigma_{a_x}^2 \end{bmatrix} \quad (5.1)$$

Steering Wheel Angle Sensor

A sensor to measure steer angles is utilized as an input since modern cars typically lack sensors to measure tire steer angles directly. In this simulation, an Ackerman steering geometry is employed with a steering ratio of $C_\delta = 21.45$ to obtain tire angle δ.

$$\delta = C_\delta * (steer\ angle) \quad (5.2)$$

Wheel Rotation Sensor

In this simulation, the wheel rotational angles are directly obtained from the dSPACE ASM vehicle dynamics model. These angles are then utilized to calculate vehicle velocity and tire slip ratios using equations presented in 4.1.2.

doi:10.6342/NTU202403171

5.3.3 Maneuvers

Double Lane Change Maneuver

The double lane change maneuver is a standardized test which assesses the handling and agility of vehicles, specifically its road-holding ability. The method is specified in [52] is applicable to vehicles weighing up to 3.5 tons gross mass. In this maneuver, the vehicle navigates through two consecutive lane changes, as seen in Figure 5-7, simulating abrupt avoidance maneuvers encountered in real-world driving situations. This test evaluates the vehicle's capability to change direction quickly while maintaining stability and control, serving as a crucial benchmark for assessing yaw dynamics.

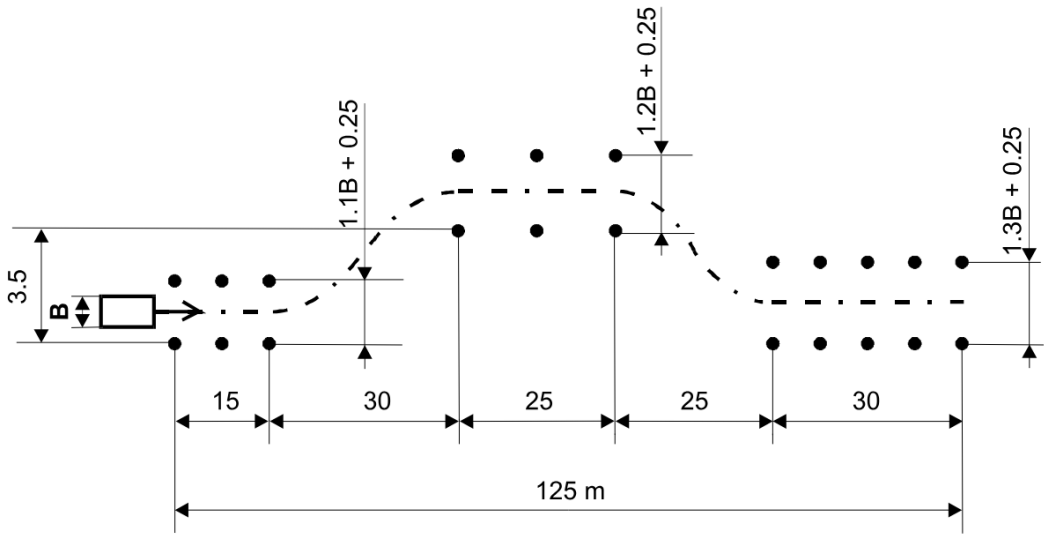

Figure 5-7 Double lane change manuever specifications [53]

doi:10.6342/NTU202403171

Constant Radius Maneuver

The constant radius maneuver, also referred to as the steady-state circular driving behavior test, is detailed in [54]. This standard applies to passenger cars and light commercial vehicles weighing up to 3.5 tons. The method includes three approaches: constant radius, constant steering angle input and constant speed, as detailed in Table 5-2 below.

Table 5-2 Variations of a steady-state steer test [54]

Test method	Constant	Variable	Measured or calculated	Variation
1	Radius	Speed	Steering wheel angle	With discrete test speeds
				With continuous speed increase
2	Steering wheel angle	Speed	Radius	With continuous speed increase
				With discrete turn radii
3	Speed	Radius	Steering-wheel angle	With discrete steering wheel angles
		Steering wheel angle	Radius	With slowly increasing steering wheel angle

In the chosen constant radius variation for this study, the maneuver proceeds as follows: the vehicle accelerates from a standstill to 15 km/h on a straight road, then enters a continuous cornering on a circular track with a constant radius of 100 meters. Finally, it accelerates further to 70 km/h before braking to a stop. The continuous velocity increase enables monitoring roll angle progression, which is crucial for assessing roll dynamics and inertial parameters. Vehicle speed is gradually increased

doi:10.6342/NTU202403171

while staying within ± 0.5 m of the desired track. The rate of lateral acceleration should increase by 0.1 m/s² per second, not exceeding 0.2 m/s² per second.

The constant radius maneuver provides a dynamic test scenario that effectively captures the wide range of vehicle roll angle, making it an ideal candidate for evaluating and refining roll dynamics estimation algorithms. While the maneuver does not represent real life driving scenarios, it remains valuable for assessing behavior of steady-state roll dynamics.

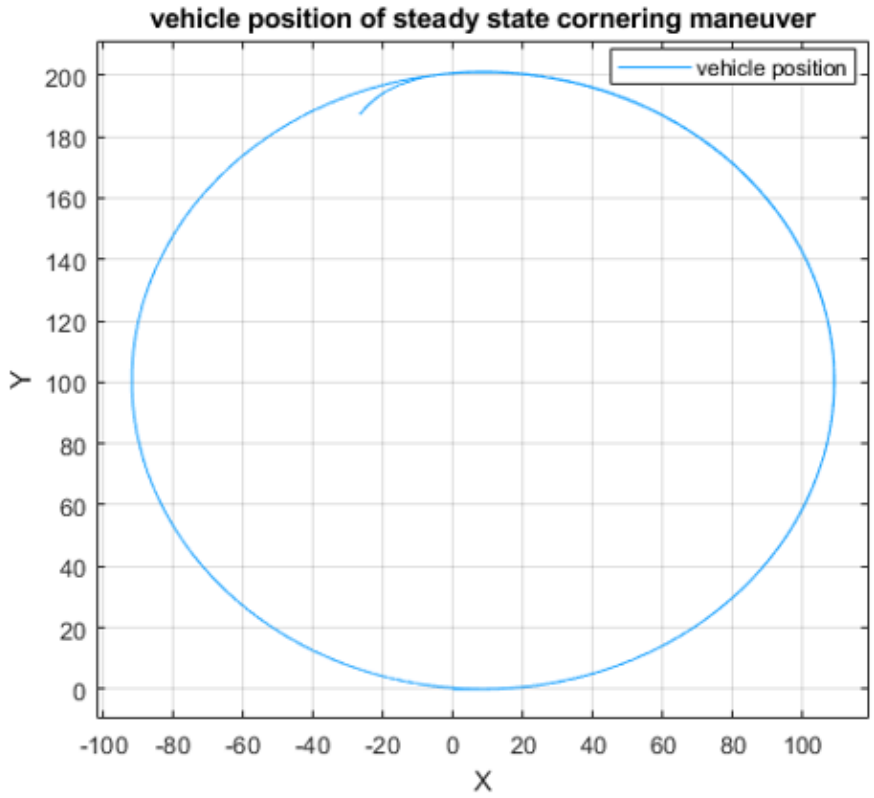

Figure 5-8 Path of the Constant Radius Maneuver

doi:10.6342/NTU202403171

Chapter 6 Results

6.1 State Estimation

The DEKF-based algorithm functions effectively as both a noise filter and a tool for virtual state sensing, using raw data as inputs. The state estimation results provide a refined and accurate depiction of the system's current state, significantly reducing noise. Additionally, unmeasurable states, such as tire forces and vehicle sideslip, are accurately obtained.

Results of state estimation are compared to actual values for both the double lane change maneuver and the constant radius maneuver. Key parameters such as longitudinal and lateral acceleration, roll and yaw rates, and sideslip angles are evaluated.

6.1.1 Longitudinal and Lateral Acceleration

The estimated values closely match the actual measured data, demonstrating the algorithm's effectiveness in accurately capturing the vehicle's dynamic response during both rapid lane changes and steadily increasing lateral acceleration. Figure 6-1 and Figure 6-2 display sensor measurements and estimations of longitudinal and lateral acceleration during the double lane change maneuver. The results demonstrate that the estimations closely align with the actual values, maintaining accuracy even

doi:10.6342/NTU202403171

during rapid cornering, aside from minor spikes observed at the initial acceleration around 2.5 seconds.

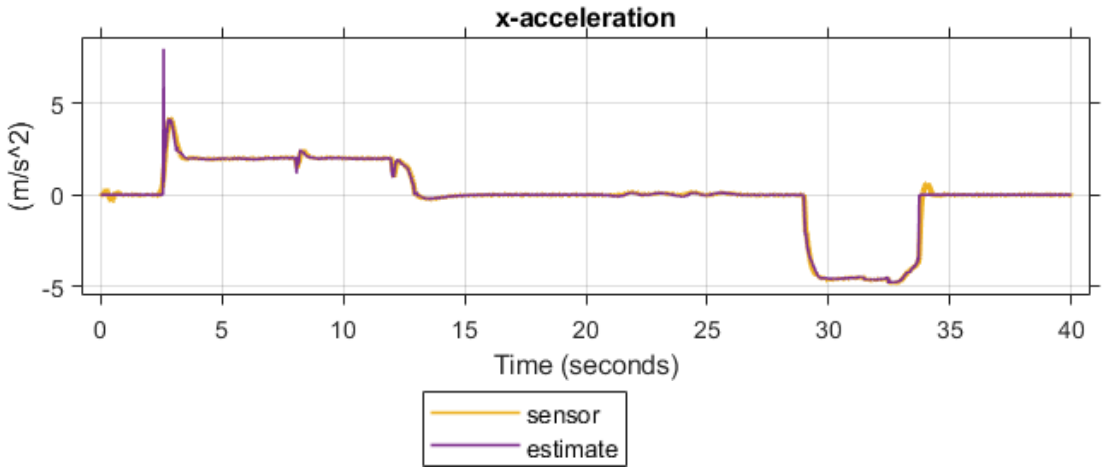

Figure 6-1 Longitudinal acceleration measurements and estimates during DLC maneuver

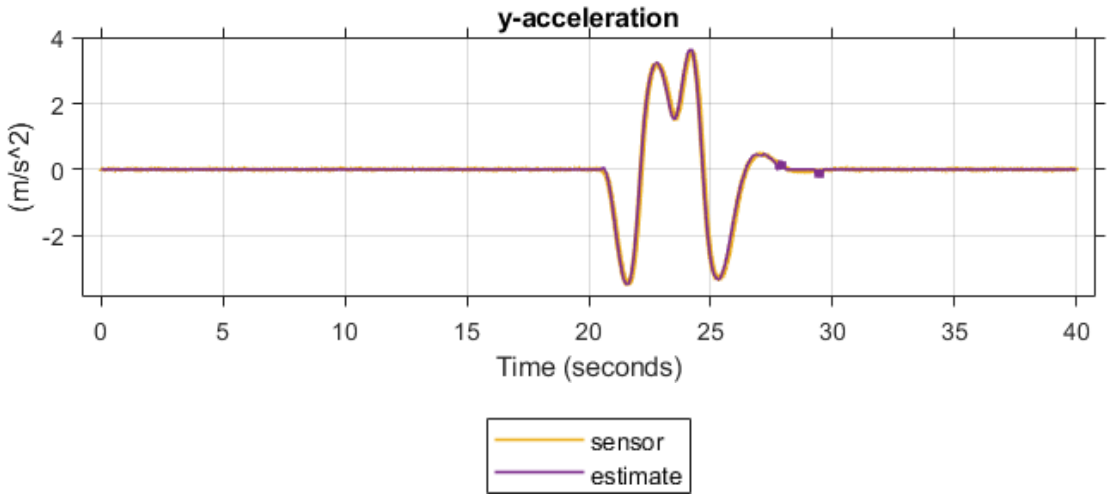

Figure 6-2 Lateral acceleration measurements and estimates during DLC maneuver

Figure 6-3 and Figure 6-4illustrate sensor measurements and estimations of longitudinal and lateral acceleration during the constant radius maneuver. Similar to the double lane change maneuver, the estimation closely matches the actual values, demonstrating consistency even under steadily increasing lateral acceleration.

doi:10.6342/NTU202403171

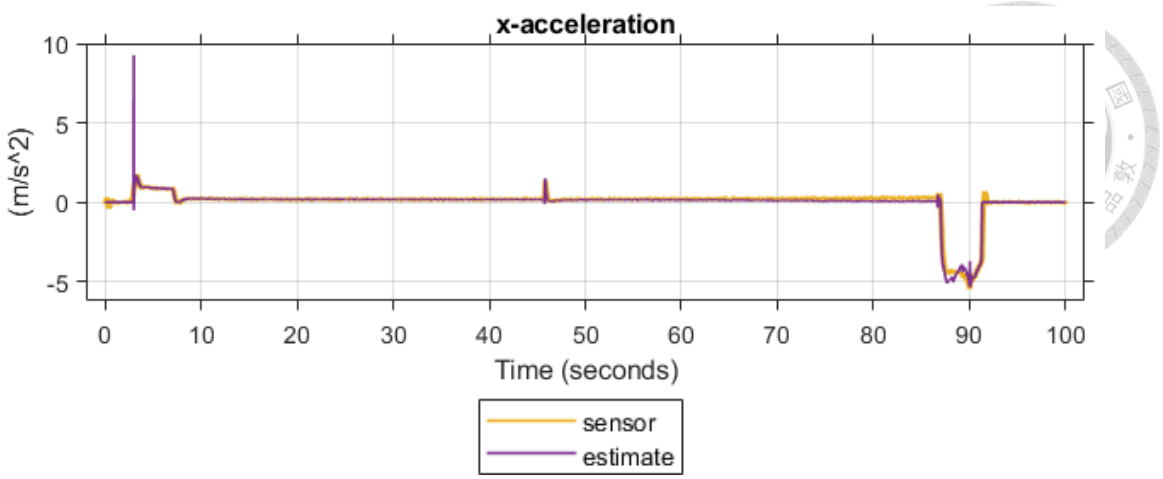

Figure 6-3 Longitudinal acceleration measurements and estimates during constant radius maneuver

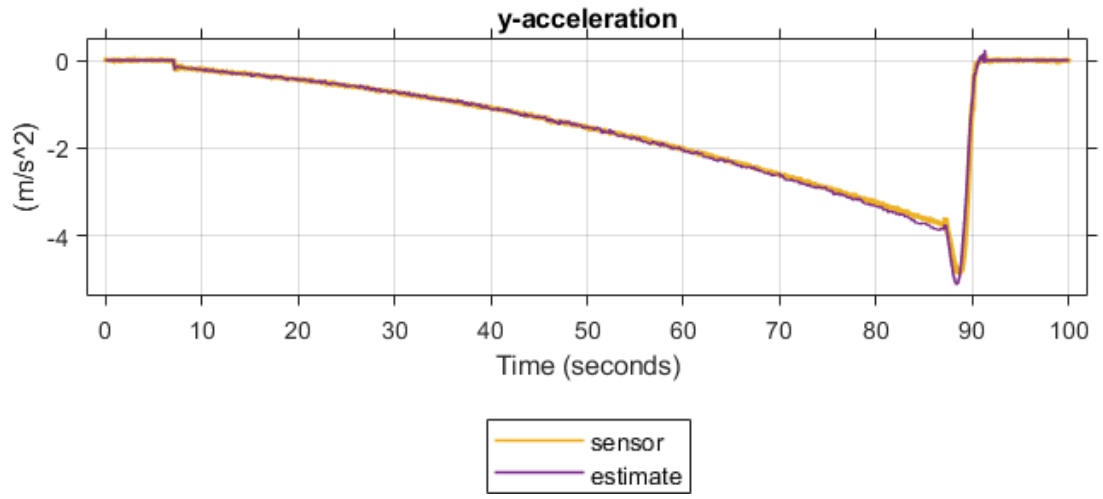

Figure 6-4 Lateral acceleration measurements and estimates during constant radius maneuver

6.1.2 Roll and Yaw Rates

The roll and yaw rate estimates perform well, effectively filtering out most of the noise to produce clean results. This demonstrates the algorithm's capability to accurately reflect the vehicle's rotational dynamics under the sudden steering inputs typical of a double lane change maneuver, as seen in Figure 6-5 and Figure 6-6, as

doi:10.6342/NTU202403171

well as during the increasing roll rate of a constant radius maneuver, depicted in Figure 6-7 and Figure 6-8.

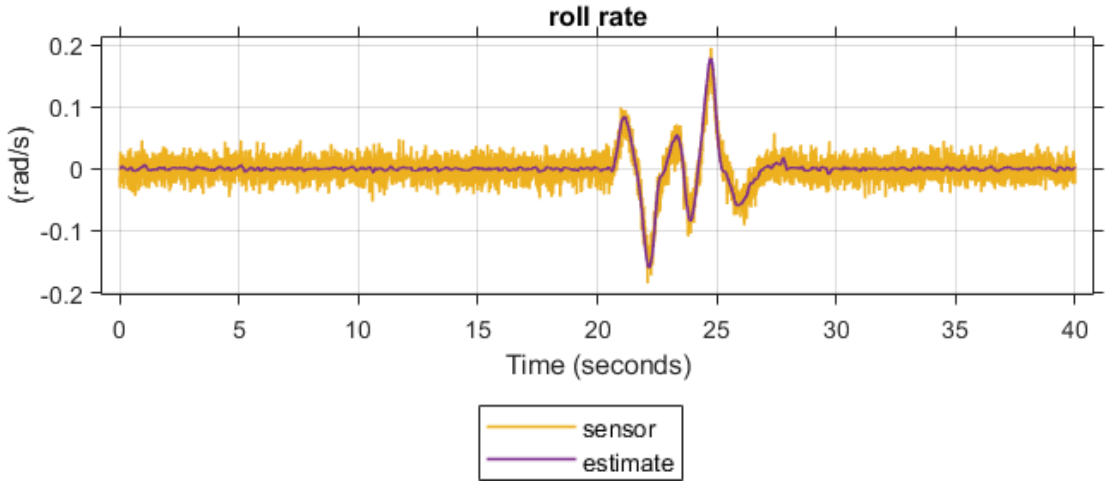

Figure 6-5 Roll rate measurements and estimates during DLC maneuver

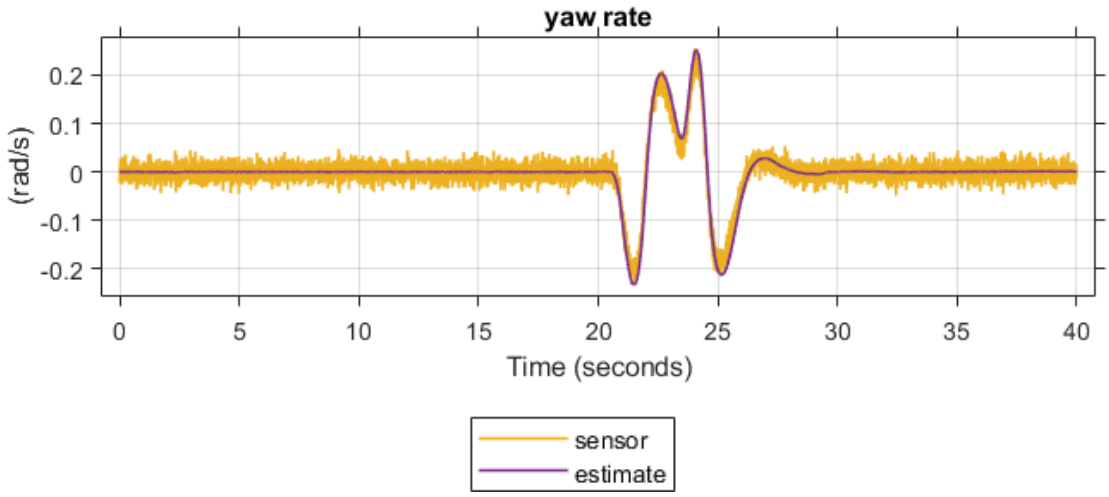

Figure 6-6 Yaw rate measurements and estimates during DLC maneuver

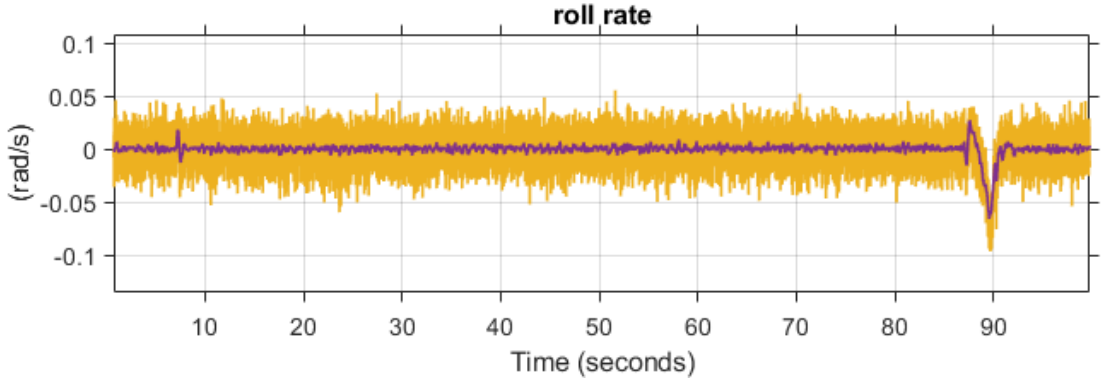

doi:10.6342/NTU202403171

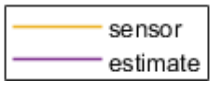

Figure 6-7 Roll rate measurements and estimates during constant radius maneuver

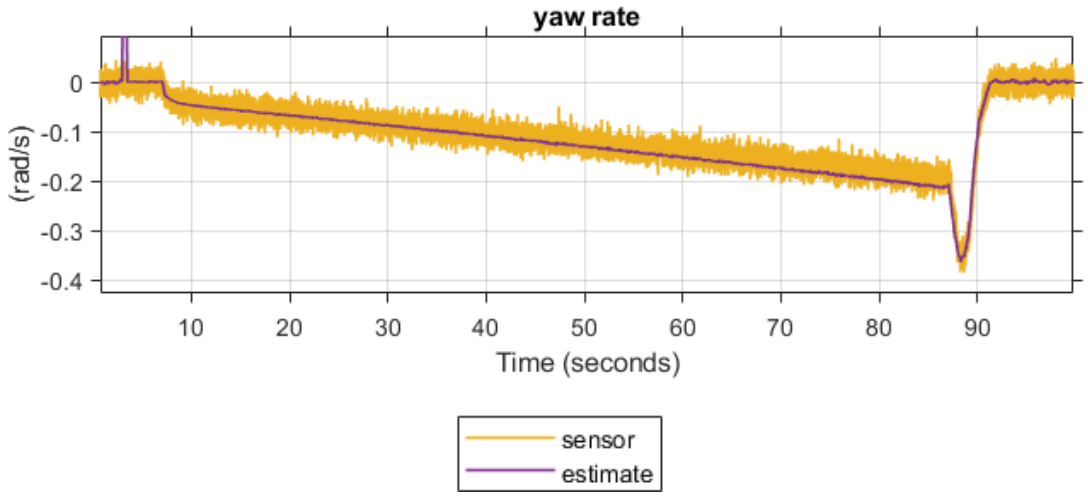

Figure 6-8 Yaw rate measurements and estimates during constant radius maneuver

6.1.3 Sideslip Angle

Unlike the previously mentioned acceleration and roll and yaw rates, the sideslip angle is not estimated directly from sensor inputs. Instead, it is calculated using system states, functioning as a virtual sensor. The sideslip angle is determined using longitudinal velocity v_x and lateral velocity v_y, as described in equation (4.13).

Figure 6-9 plots sideslip angle estimates alongside actual values during the double lane change maneuver, illustrating that when the vehicle is in motion, the estimator approximates values and trends similarly to the actual sideslip obtained in dSPACE. Similarly, in the constant radius maneuver depicted in Figure 6-10,

doi:10.6342/NTU202403171

estimated sideslip angles closely track the actual values throughout most of the maneuver, with slight deviation observed during braking.

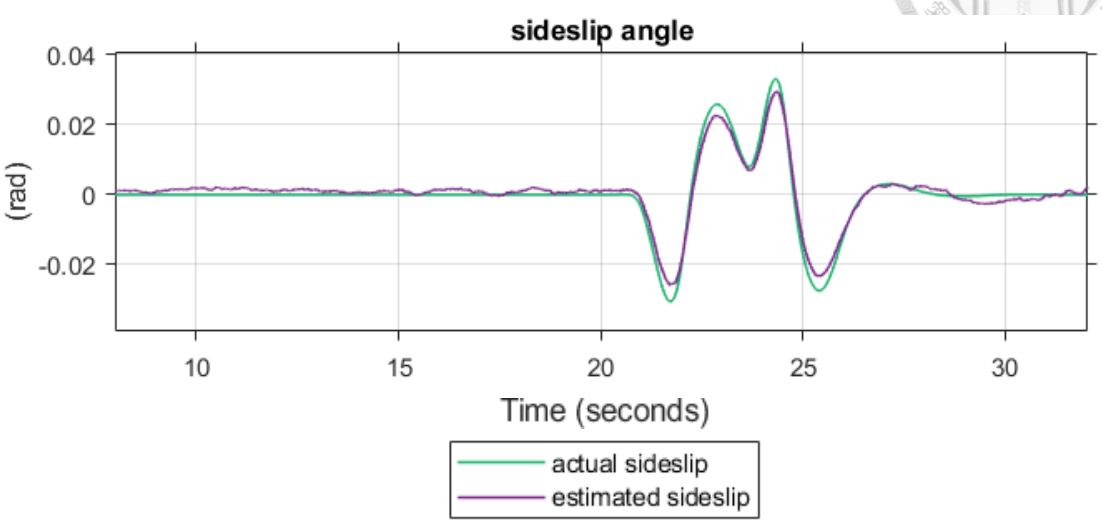

Figure 6-9 Sideslip angle estimates during double lane change manuever

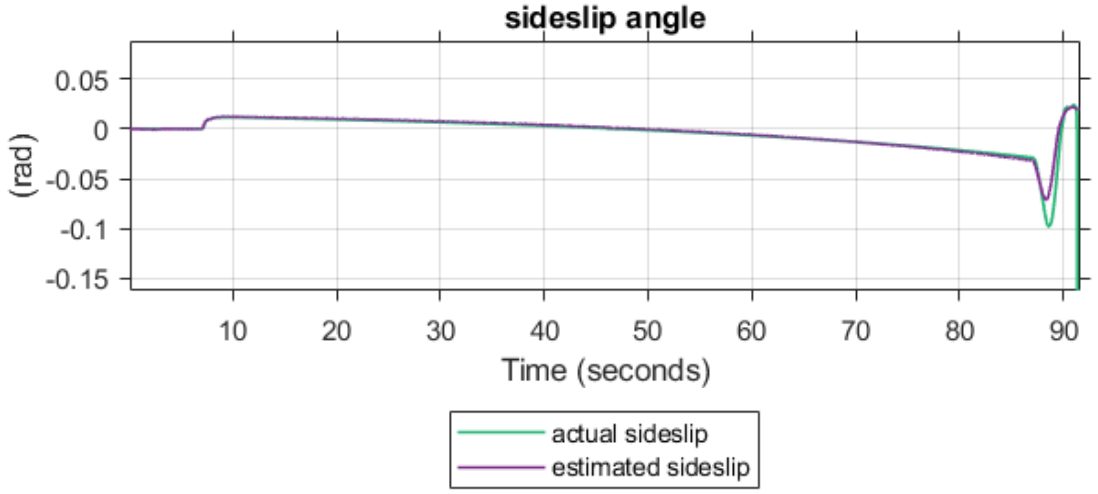

Figure 6-10 Sideslip angle estimates during constant radius manuever

Overall, the state estimation results for both the double lane change and constant radius maneuvers demonstrate the dual estimation framework's ability to accurately identify vehicle states, effectively fulfilling its primary role as a state estimator.

doi:10.6342/NTU202403171

6.2 Parameter Identification

The purpose of the proposed algorithm is to obtain parameter estimates for different loading vehicles, aiming to refine the model outputs until they closely match the observed data. The results of parameter estimation offer insights into system changes. Three test cases are compared: an unladen vehicle, and conditions with additional loads of $m_a = 500\,\text{kg}$ and $1500\,\text{kg}$. The parameters considered include mass, center of gravity longitudinal position and height, and roll and yaw moments of inertia.

6.2.1 Mass Estimates

In Figure 6-11, the mass estimated during a DLC maneuver is shown. The plot shows the actual and estimated masses across different loading conditions, with the estimates converging to values closer to the actual mass. In this simulation, the results for loads of 1500 kg, 500 kg, and 0 kg are within 1.2%, 4.4%, and 12.6% of the actual parameters, respectively. These findings underscore the algorithm's effectiveness in accurately estimating parameters and faithfully reflecting the system's true dynamics.

doi:10.6342/NTU202403171

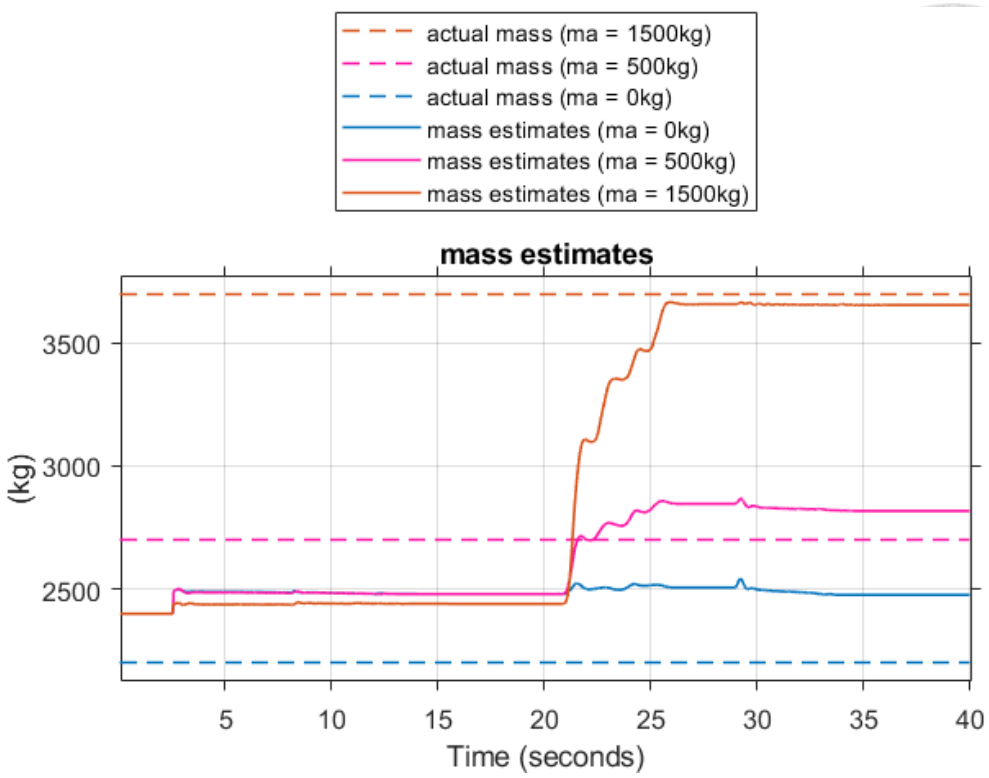

Figure 6-11 Vehicle mass estimates during double lane change manuever

Figure 6-12 and Figure 6-13 illustrate the estimated and actual values of COG position and moments of inertia for the three loading conditions. The graphs show the estimated and actual COG longitudinal position and height, with estimated values errors within 3.2% and 14.7% of actual values, respectively. The alignment of these values demonstrates the accuracy of the parameter estimation process.

doi:10.6342/NTU202403171

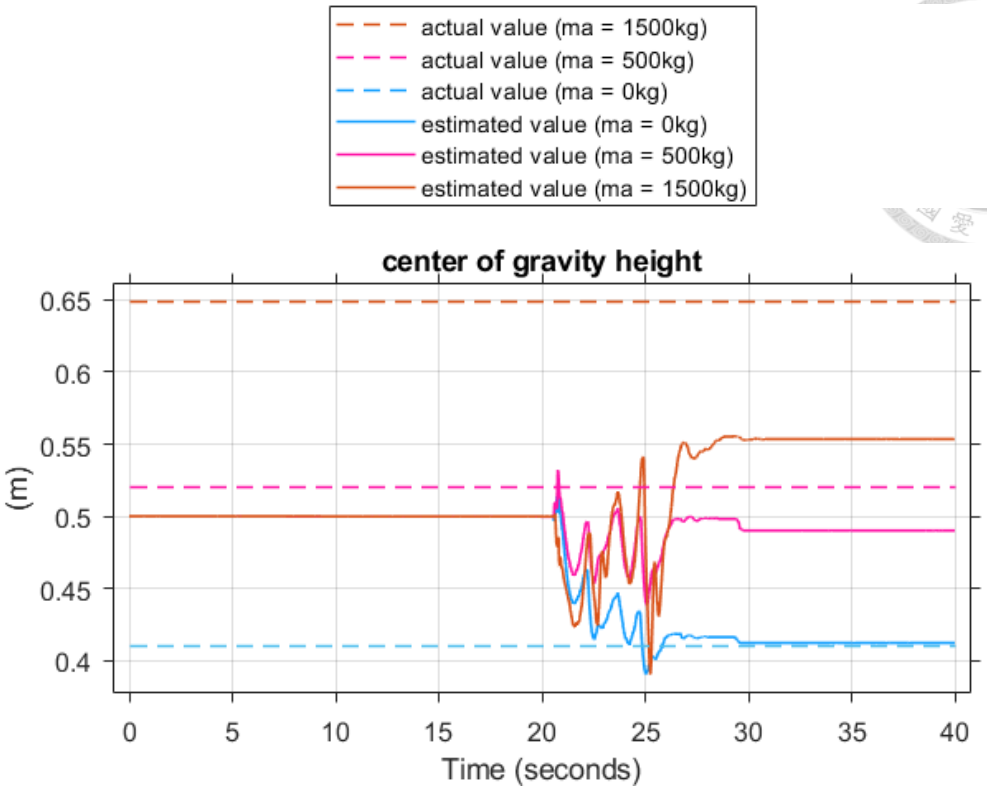

Figure 6-12 COG height estimates during DLC manuever

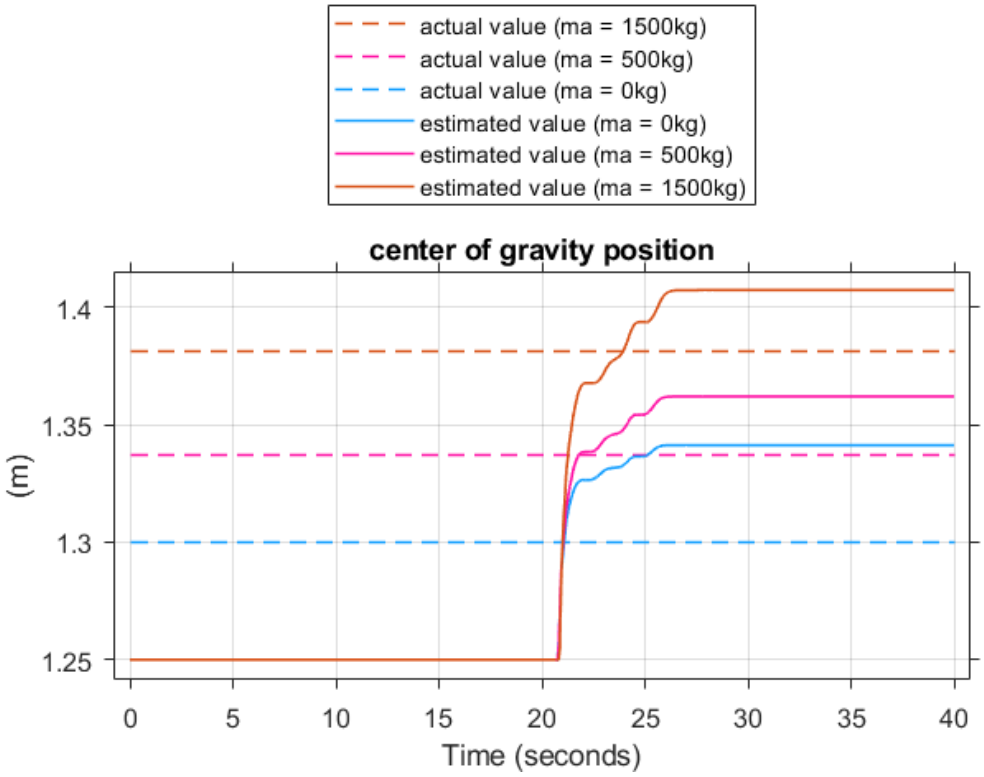

Figure 6-13 COG longitudinal position estimates during DLC manuever

doi:10.6342/NTU202403171

6.2.2 Inertial Parameter Estimates

Figure 6-14 and Figure 6-18 display the estimated and actual values of moments of inertia about x and z axes, capturing the inertial properties by relating the parameters as described in Section 4.3.2. Since these values compound the errors in both mass and COG position estimates, yaw and roll moments of inertia are within 13.7% and 9.6% of actual values, respectively.

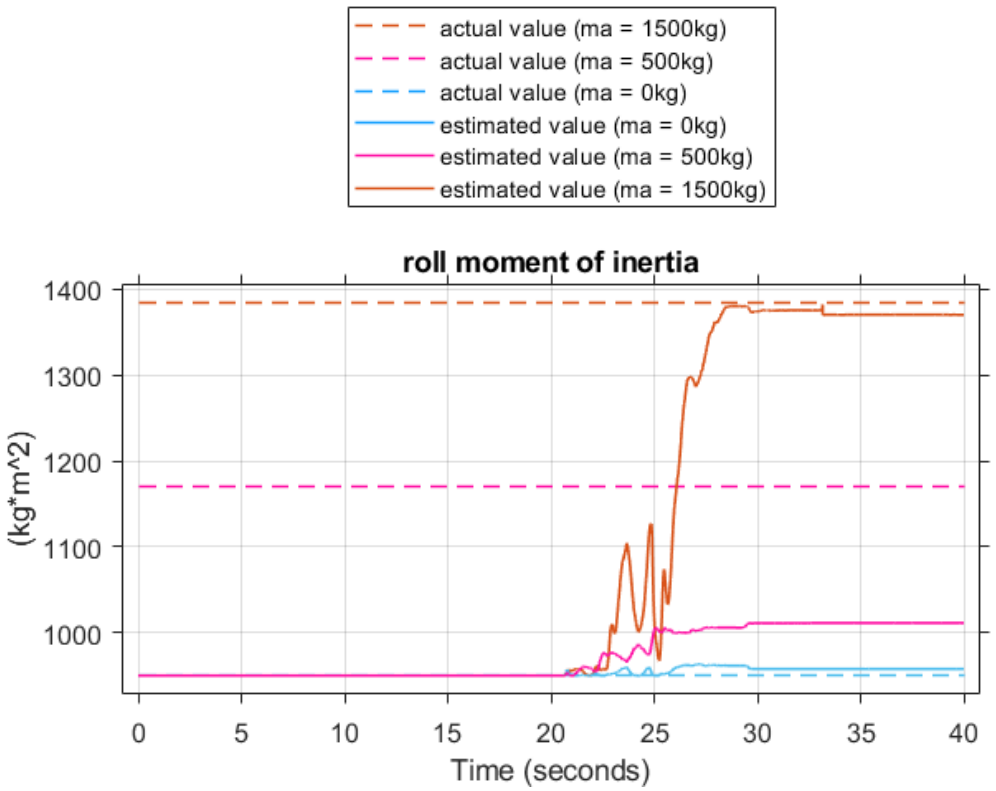

Figure 6-14 Roll moment of inertia estimates during DLC manuever

doi:10.6342/NTU202403171

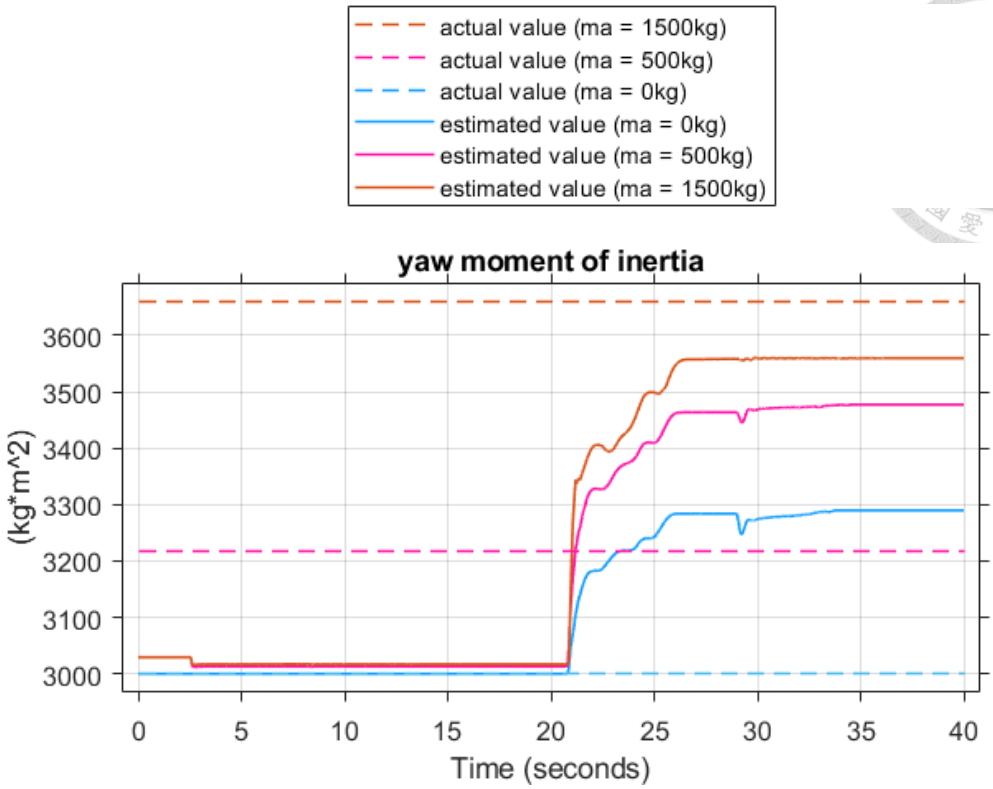

Figure 6-15 Yaw moment of inertia estimates during DLC manuever

6.3 State Estimation with Parameter Update

State estimation before and after parameter updates involves comparing the accuracy of state estimates using initial parameter values versus updated ones. Post-parameter estimation, the updated values are used in the state estimation process, typically leading to more accurate and reliable state estimates.

In this analysis, we compare the estimated states to ground truth data to verify that with parameter updates, the state estimation outperforms a standard state estimator, better reflecting the system's true dynamics. The cases considered include scenarios where additional loads are 1500 kg.

doi:10.6342/NTU202403171

6.3.1 Double Lane Change Maneuver

During the double lane change maneuver, the estimator with parameter updates demonstrates significantly improved performance. Figure 6-16 compares longitudinal acceleration estimates with actual values, demonstrating minimal error due to high estimation accuracy even without parameter updates. Figure 6-17 compares the lateral acceleration, revealing a reduction in root mean square (RMS) error by 0.0649 m/s², representing a 44.6% improvement.

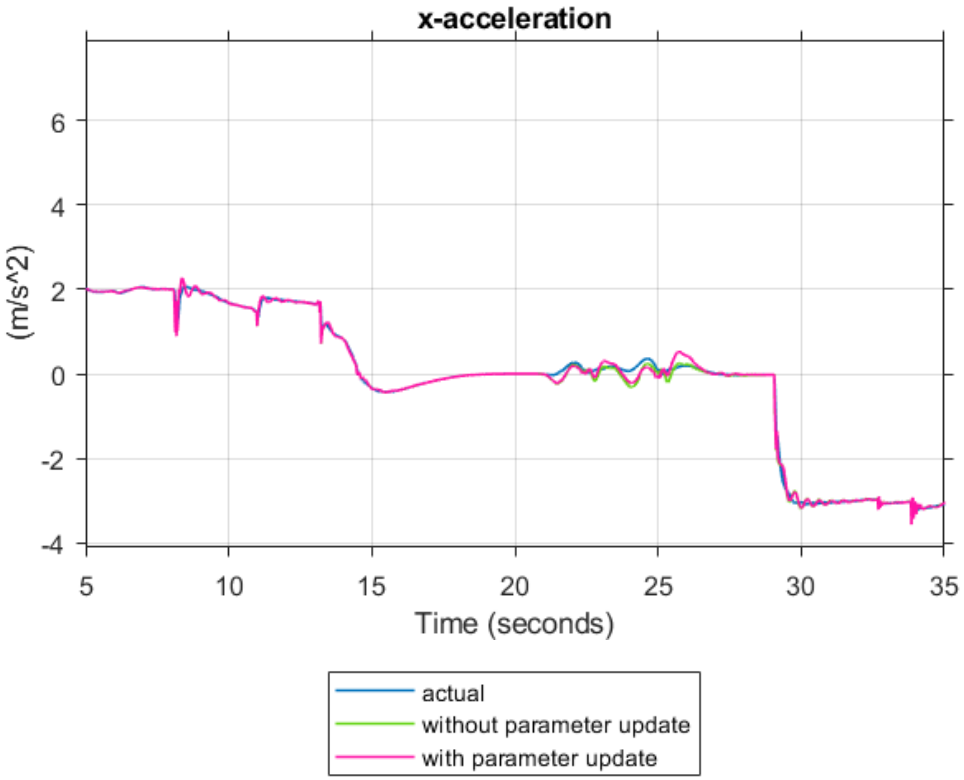

Figure 6-16 Longitudinal acceleration estimates during DLC manuever

doi:10.6342/NTU202403171

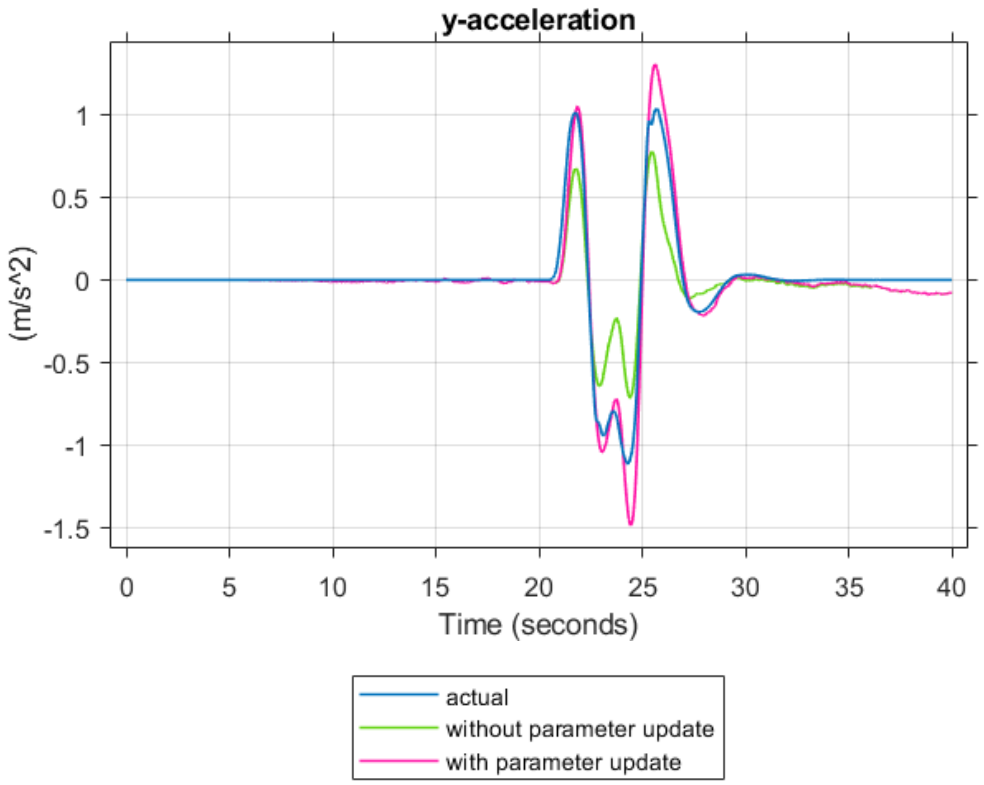

Figure 6-17 Lateral acceleration estimates during DLC manuever

Figure 6-18 indicates that the yaw rate estimation is reduced with parameter updates, leading to an increase in RMS error of 0.00105 rad/s. This discrepancy may be attributed to the previously observed underestimation of the moment of inertia about the z-axis, as shown in Figure 6-15.

doi:10.6342/NTU202403171

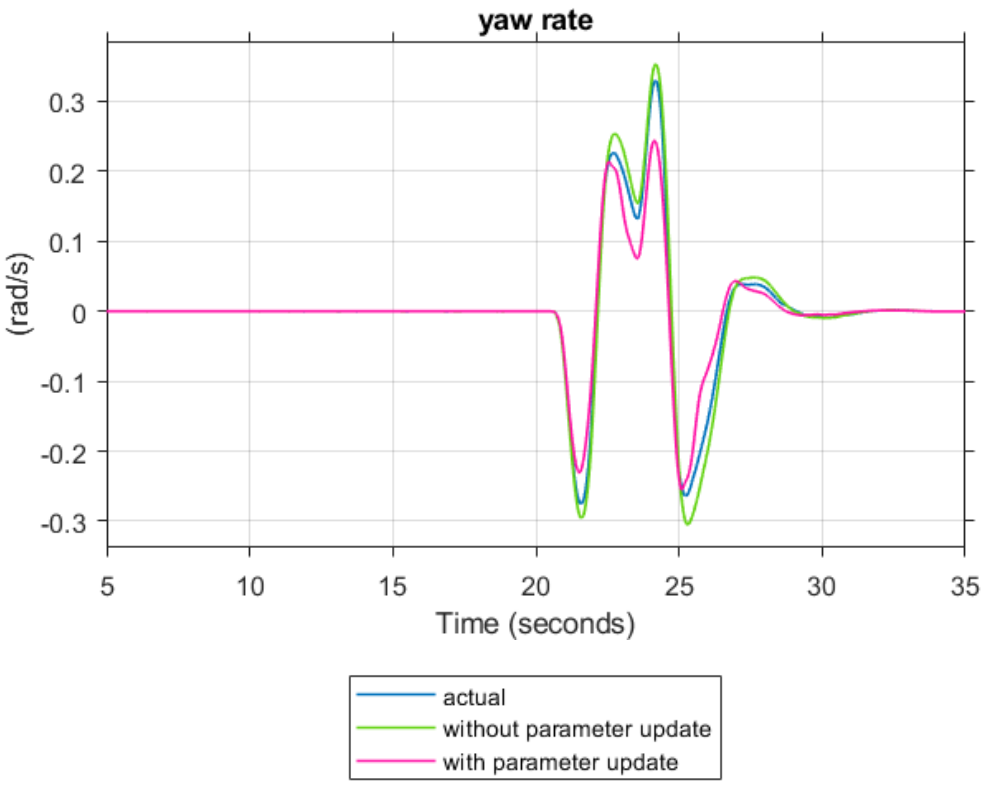

Figure 6-18 Yaw rate estimates during DLC manuever

Figure 6-19, Figure 6-20 and Figure 6-21 illustrate significant reductions in errors for roll rate, roll angles, and vehicle sideslip angle, with decreased RMS errors of 0.0088 rad/s, 0.0199 rad, and 0.0091 rad. The RMS errors of vehicle states are organized and presented in Table 6.1. These improvements correspond to reductions in RMS error by 44.6%, 44.2%, and 65.4%, respectively. These enhancements in key vehicle states highlight the considerable accuracy improvements achieved through parameter updates in state estimation.

doi:10.6342/NTU202403171

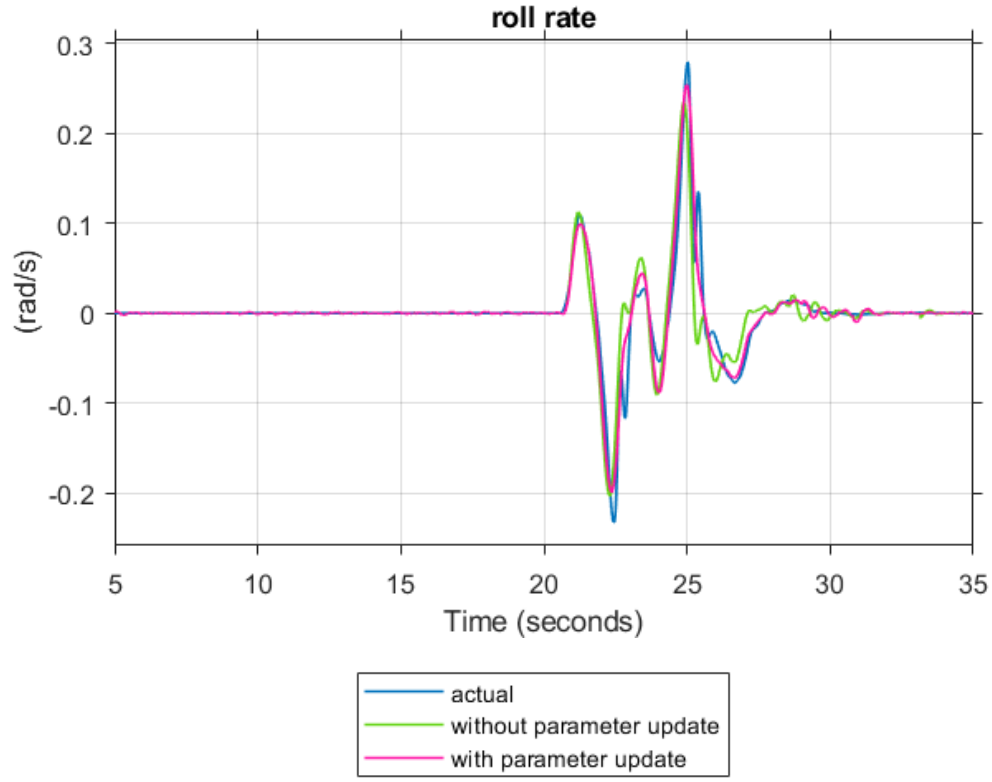

Figure 6-19 Roll rate estimates during DLC manuever

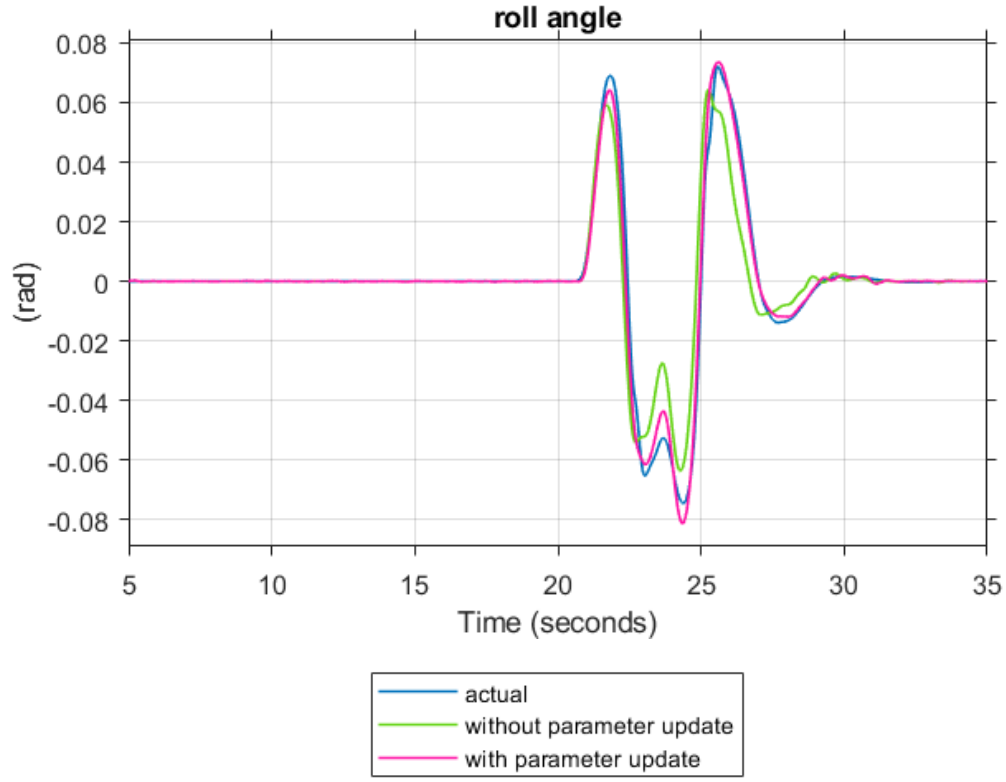

Figure 6-20 Roll angle estimates during DLC manuever

doi:10.6342/NTU202403171

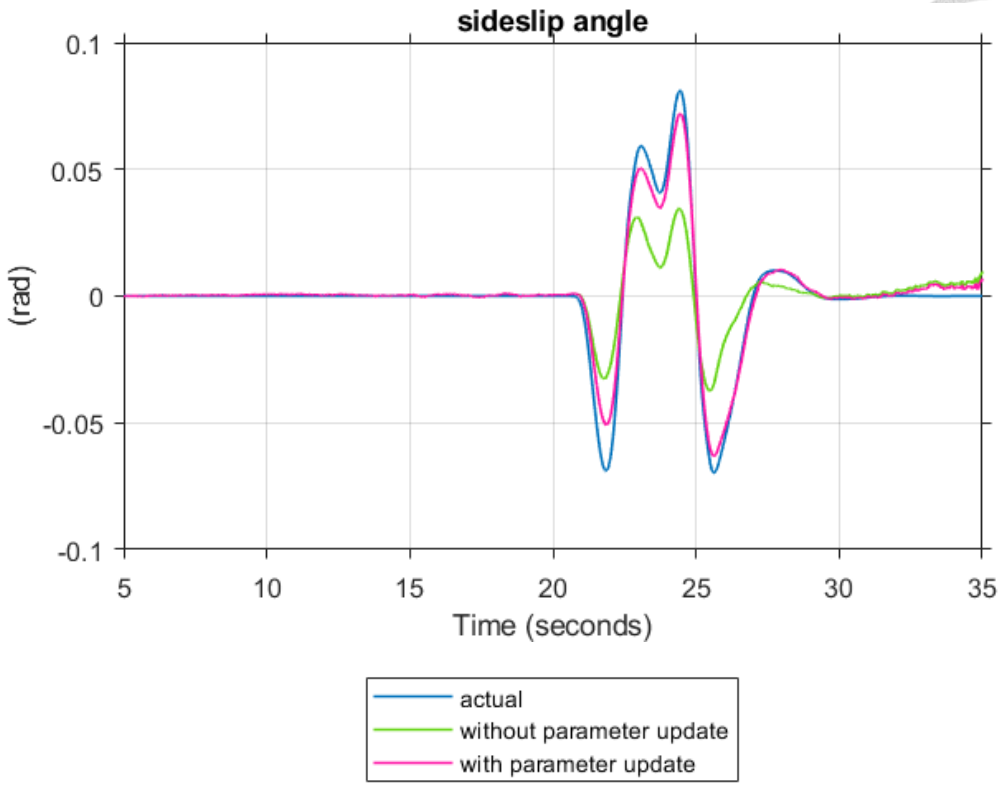

Figure 6-21 Sideslip angle estimates during DLC manuever

Table 6-1 RMS error of states of DLC maneuver

	Without Update	**With Update**	Improvement(%)
$a_x(m/s^2)$	0.1773	0.1772	0.056
$a_y(m/s^2)$	0.1454	0.0805	44.64
$\dot{\phi}(rad/s)$	0.0199	0.0111	44.22
$\phi(rad)$	0.0081	0.0028	65.43
$\dot{\psi}(rad/s)$	0.0200	0.0305	-52.5
$\beta(rad)$	0.0130	0.0039	70

doi:10.6342/NTU202403171

6.3.2 Constant Radius Maneuver

The effectiveness of parameter updates on state estimation during a constant radius maneuver is evident from the RMS error comparisons. Without parameter updates, the RMS errors were significantly higher, as shown in Table 6-2.

Figure 6-22 compares longitudinal acceleration estimates with actual values during the constant radius maneuver. Following parameter updates, reductions in RMS errors were observed: longitudinal acceleration decreased by 0.1947 m/s², indicating a 29.7% improvement.

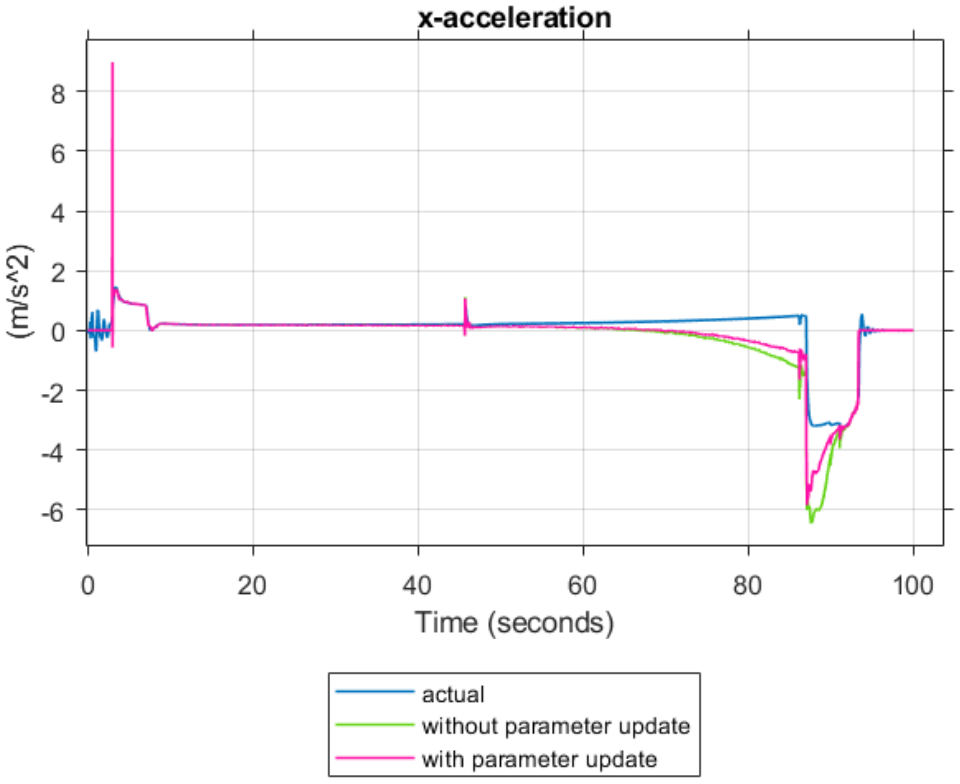

Figure 6-22 Longitudinal acceleration estimates during constant radius manuever

doi:10.6342/NTU202403171

Figure 6-23 illustrates the comparison of lateral acceleration during the constant radius maneuver, with an RMS error reduction of 0.2457 m/s², representing a decrease of 56.6%. In Figure 6-24, the comparison of yaw rate indicates an RMS decrease of 0.0280 rad/s, marking a reduction of 28.9%.

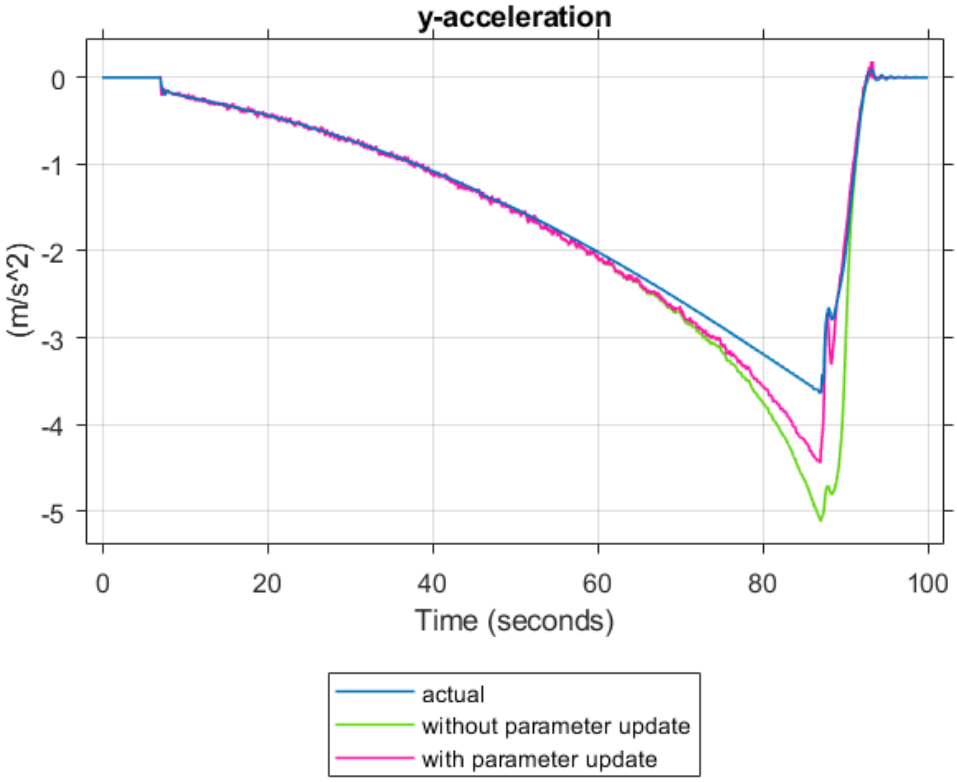

Figure 6-23 Lateral acceleration estimates during constant radius manuever

doi:10.6342/NTU202403171

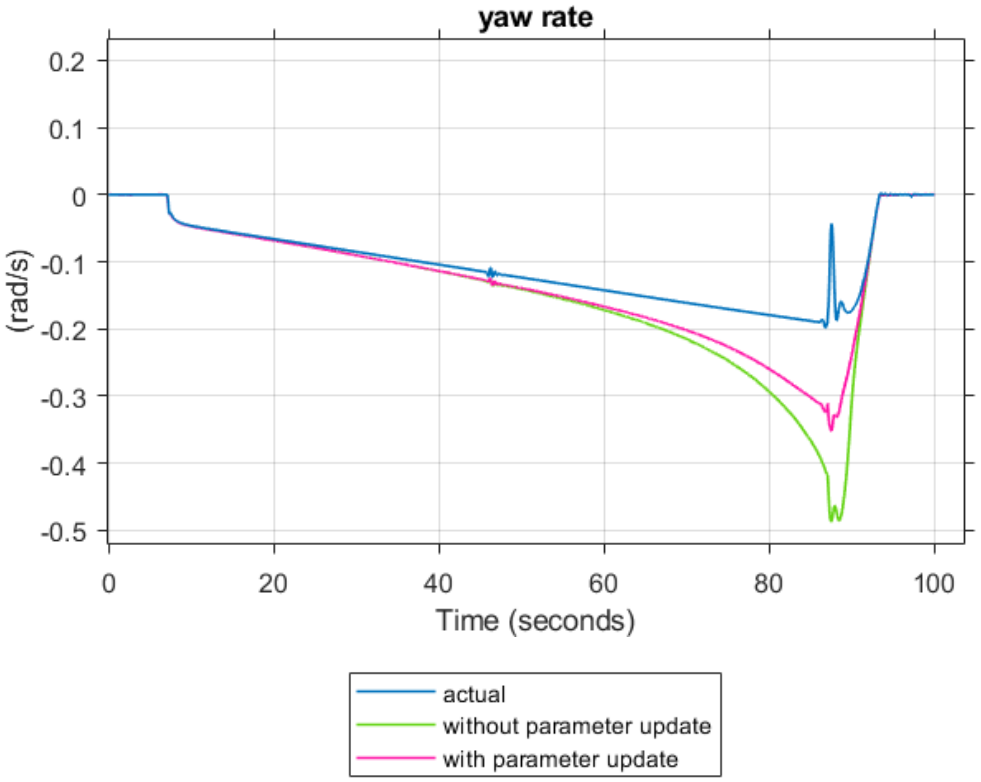

Figure 6-24 Yaw rate estimates during constant radius manuever

While enhancements in roll dynamics and vehicle sideslip were moderate, as presented in Table 6.2, the overall results nonetheless offer a more accurate representation of the vehicle's dynamics. The less pronounced improvement can be attributed to the parameter update being computed based on the discrepancy between measurements and state estimation, as illustrated in Figure 6.7, where improvement are minimal during steady increases in vehicle dynamics, as observed in roll rates (Figure 6-26) and sideslip angles (Figure 6-27). Thus, the proposed method may exhibit limitations under such conditions.

doi:10.6342/NTU202403171

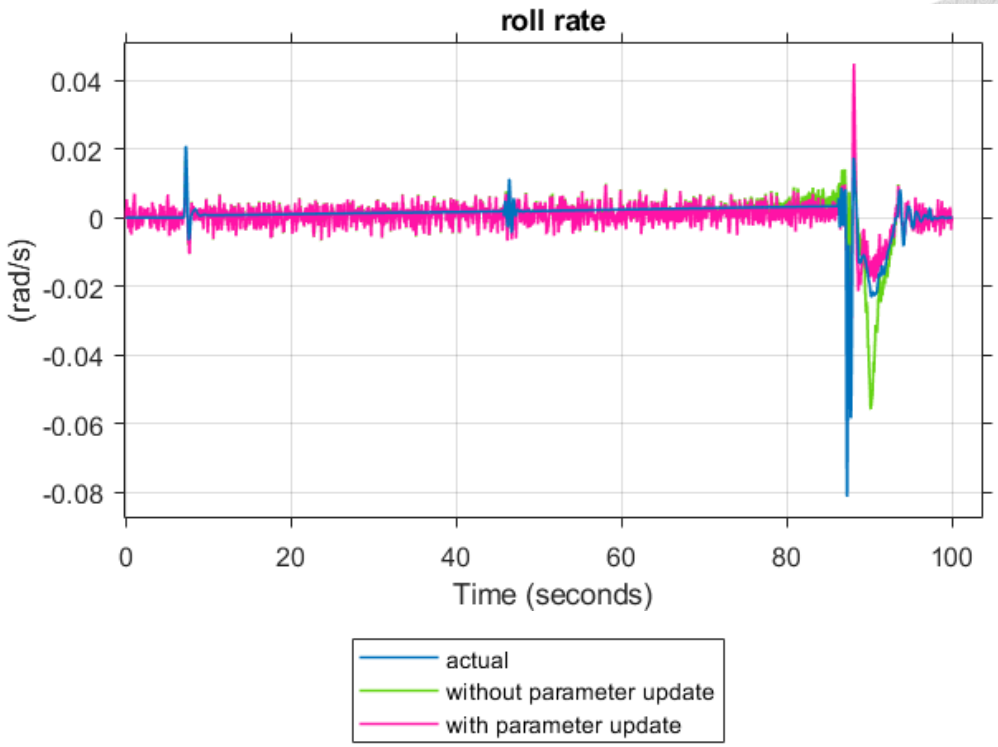

Figure 6-25 Roll rate estimates during constant radius manuever

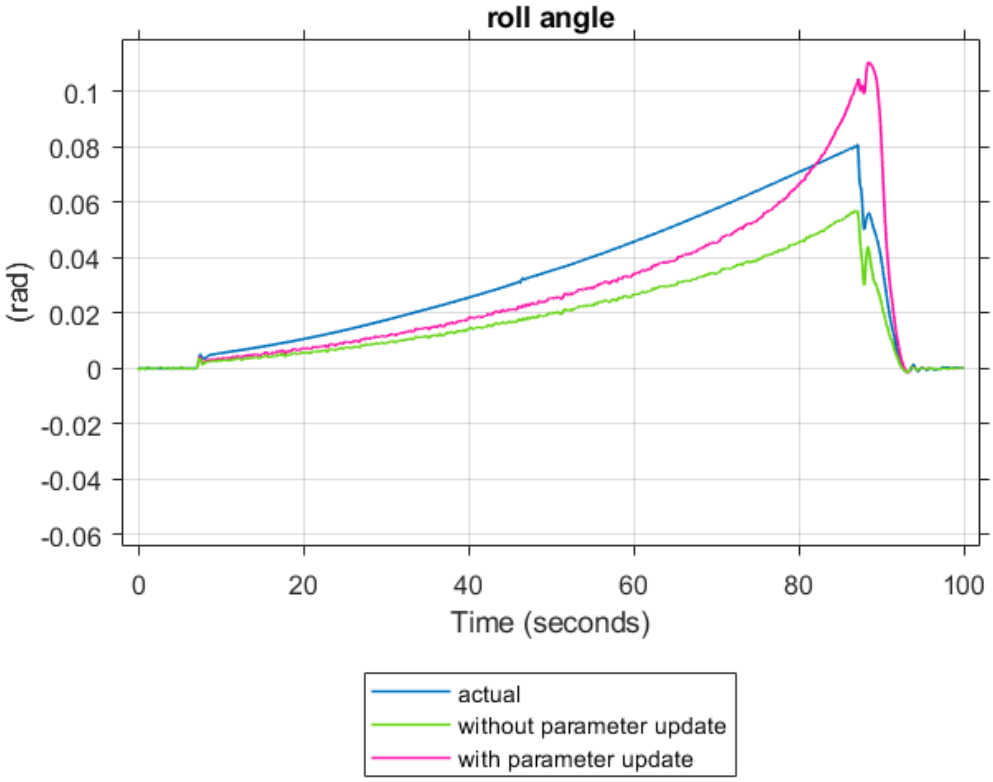

Figure 6-26 Roll angle estimates during constant radius manuever

doi:10.6342/NTU202403171

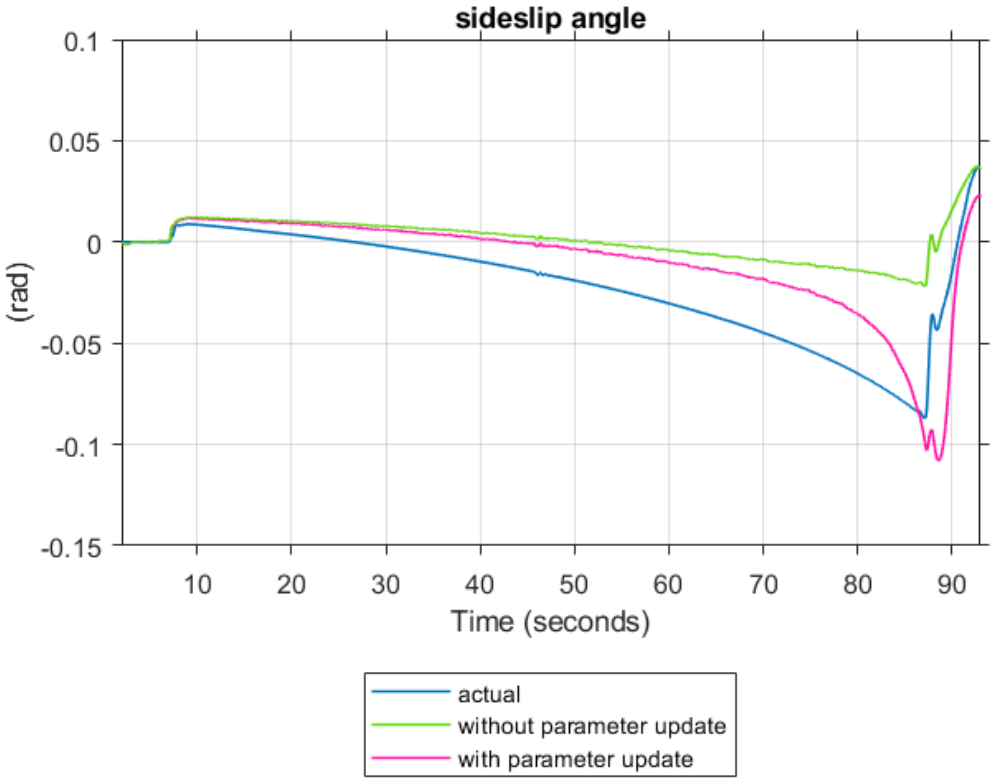

Figure 6-27 Sideslip estimates during constant radius manuever

Table 6-2 RMS error of states of constant radius maneuver

	Without Update	**With Update**	Improvement(%)
$a_x(m/s^2)$	0.6560	0.4613	29.68
$a_y(m/s^2)$	0.4344	0.1887	56.56
$\dot{\phi}(rad/s)$	0.0045	0.0032	28.89
$\phi(rad)$	0.0149	0.0118	20.81
$\dot{\psi}(rad/s)$	0.0743	0.0463	37.69
$\beta(rad)$	0.2477	0.2443	1.37

doi:10.6342/NTU202403171

Chapter 7 Conclusions and Future Work

7.1 Conclusions

In this thesis, we propose a real-time state and parameter estimation method targeting load-carrying vehicles employing a Dual Extended Kalman Filter approach. This method operates by running state estimation and parameter identification processes in parallel, enabling real-time tracking of dynamic states and updates of vehicle system inertial parameters.

Simulation results indicate that the DEKF can estimate inertial parameters of a vehicle under various load conditions, with parameters estimated within 15% of actual values. The DEKF also significantly improves the accuracy of vehicle state estimation. During the constant radius maneuver, the RMS error for longitudinal acceleration decreased from 0.6560 m/s^2 to 0.4613 m/s^2, and for lateral acceleration, from 0.4344 m/s^2 to 0.1887 m/s^2. In the double lane change maneuver, the RMS error for lateral acceleration decreased from 0.1454 m/s^2 to 0.0805 m/s^2, while roll rate errors improved from 0.0199 rad/s to 0.0111 rad/s.

These findings demonstrate the DEKF's efficacy in accurately capturing changes in vehicle dynamics under different loading scenarios, marking a significant advancement over conventional estimation techniques.

doi:10.6342/NTU202403171

7.2 Future Works

While the algorithm proposed has significantly advanced real-time state and parameter estimation for load-carrying vehicles, several areas offer potential for further exploration:

1. Extend Model Complexity

Future work could enhance the current model by incorporating more complex vehicle dynamics, such as increasing the number of DOFs to accommodate additional states and movements. Additionally, including external factors like tire-road characteristics or accounting for tire degradation would improve the robustness and applicability of the estimator across diverse environments.

2. Adaptive Filtering Techniques

Incorporating advanced filtering techniques, such as the UKF or AKF, could further enhance the performance of the Dual Kalman Filter framework. The UKF can better handle nonlinear systems, while adaptive filtering techniques can dynamically adjust parameters in response to changing system dynamics and measurement noise characteristics, enhancing the overall precision and reliability of the estimator.

doi:10.6342/NTU202403171

3. Integration with Vehicle Control Systems

Integrating the proposed state estimation and parameter identification framework with advanced driver assistance systems, such as stability control and rollover prevention, could provide a comprehensive solution for real-time vehicle control.

4. Real-world Testing and Validation

While this research has been fully conducted in simulation, it is crucial to perform real-world testing and validation in various scenarios to further verify efficacy and reliability of the suggested approach. Real-world experiments will provide insights into the algorithm's performance and applicability under actual conditions.

doi:10.6342/NTU202403171

References

[1] N. H. T. S. Administration, "Traffic safety facts 2021: A compilation of motor vehicle traffic crash data," National Center for Statistics and Analysis, 2023.

[2] B.-C. Chen and F.-C. Hsieh, "Sideslip angle estimation using extended Kalman filter," *Vehicle System Dynamics,* vol. 46, no. S1, pp. 353-364, 2008.

[3] R. Rajamani, D. Piyabongkarn, V. Tsourapas, and J. Y. Lew, "Parameter and State Estimation in Vehicle Roll Dynamics," *IEEE Transactions on Intelligent Transportation Systems,* vol. 12, no. 4, pp. 1558-1567, 2011, doi: 10.1109/tits.2011.2164246.

[4] R. Rajamani, D. Piyabongkarn, V. Tsourapas, and J. Y. Lew, "Real-time estimation of roll angle and CG height for active rollover prevention applications," in *2009 American Control Conference*, 10-12 June 2009 2009, pp. 433-438, doi: 10.1109/ACC.2009.5160045.

[5] H. Guo, D. Cao, H. Chen, C. Lv, H. Wang, and S. Yang, "Vehicle dynamic state estimation: state of the art schemes and perspectives," *IEEE/CAA Journal of Automatica Sinica,* vol. 5, no. 2, pp. 418-431, 2018, doi: 10.1109/JAS.2017.7510811.

[6] E. Narby, "Modeling and estimation of dynamic tire properties," Institutionen för systemteknik, 2006.

[7] T. A. Wenzel, K. J. Burnham, M. V. Blundell, and R. A. Williams, "Dual extended Kalman filter for vehicle state and parameter estimation," *Vehicle System Dynamics,* vol. 44, no. 2, pp. 153-171, 2006, doi: 10.1080/00423110500385949.

[8] K. Tin Leung, J. F. Whidborne, D. Purdy, and A. Dunoyer, "A review of ground vehicle dynamic state estimations utilising GPS/INS," *Vehicle System Dynamics,* vol. 49, no. 1-2, pp. 29-58, 2011.

[9] K. B. Singh, M. A. Arat, and S. Taheri, "Literature review and fundamental approaches for vehicle and tire state estimation," *Vehicle System Dynamics,* vol. 57, no. 11, pp. 1643-1665, 2018, doi: 10.1080/00423114.2018.1544373.

[10] W. Cho, J. Yoon, S. Yim, B. Koo, and K. Yi, "Estimation of tire forces for application to vehicle stability control," *IEEE Transactions on Vehicular Technology,* vol. 59, no. 2, pp. 638-649, 2009.

doi:10.6342/NTU202403171

[11] X. Jin and G. Yin, "Estimation of lateral tire–road forces and sideslip angle for electric vehicles using interacting multiple model filter approach," *Journal of the Franklin Institute,* vol. 352, no. 2, pp. 686-707, 2015.

[12] G. Baffet, A. Charara, and D. Lechner, "Estimation of vehicle sideslip, tire force and wheel cornering stiffness," *Control Engineering Practice,* vol. 17, no. 11, pp. 1255-1264, 2009.

[13] Y. Aoki, T. Inoue, and Y. Hori, "Robust design of gain matrix of body slip angle observer for electric vehicles and its experimental demonstration," in *The 8th IEEE International Workshop on Advanced Motion Control, 2004. AMC'04.*, 2004: IEEE, pp. 41-45.

[14] J. Farrelly and P. Wellstead, "Estimation of vehicle lateral velocity," in *Proceeding of the 1996 IEEE International Conference on Control Applications IEEE International Conference on Control Applications held together with IEEE International Symposium on Intelligent Contro*, 1996: IEEE, pp. 552-557.

[15] D. Piyabongkarn, R. Rajamani, J. A. Grogg, and J. Y. Lew, "Development and experimental evaluation of a slip angle estimator for vehicle stability control," *IEEE Transactions on control systems technology,* vol. 17, no. 1, pp. 78-88, 2008.

[16] M. Tanelli, S. M. Savaresi, and C. Cantoni, "Longitudinal vehicle speed estimation for traction and braking control systems," in *2006 IEEE Conference on Computer Aided Control System Design, 2006 IEEE International Conference on Control Applications, 2006 IEEE International Symposium on Intelligent Control*, 2006: IEEE, pp. 2790-2795.

[17] L. Chu, Y. Shi, Y. Zhang, H. Liu, and M. Xu, "Vehicle lateral and longitudinal velocity estimation based on Adaptive Kalman Filter," in *2010 3rd International Conference on Advanced Computer Theory and Engineering (ICACTE)*, 2010, vol. 3: IEEE, pp. V3-325-V3-329.

[18] L. Chu, L. Chao, Y. Zhang, and Y. Shi, "Design of longitudinal vehicle velocity observer using fuzzy logic and Kalman filter," in *Proceedings of 2011 International Conference on Electronic & Mechanical Engineering and Information Technology*, 2011, vol. 6: IEEE, pp. 3225-3228.

[19] C. Larish, D. Piyabongkarn, V. Tsourapas, and R. Rajamani, "A New Predictive Lateral Load Transfer Ratio for Rollover Prevention Systems," *IEEE*

doi:10.6342/NTU202403171

Transactions on Vehicular Technology, vol. 62, no. 7, pp. 2928-2936, 2013, doi: 10.1109/tvt.2013.2252930.

[20] H. Yue, L. Zhang, H. Shan, H. Liu, and Y. Liu, "Estimation of the vehicle's centre of gravity based on a braking model," *Vehicle System Dynamics,* vol. 53, no. 10, pp. 1520-1533, 2015, doi: 10.1080/00423114.2015.1064971.

[21] M. Rozyn and N. Zhang, "A method for estimation of vehicle inertial parameters," *Vehicle System Dynamics,* vol. 48, no. 5, pp. 547-565, 2010, doi: 10.1080/00423110902939863.

[22] S. Solmaz, M. Akar, R. Shorten, and J. Kalkkuhl, "Real-time multiple-model estimation of centre of gravity position in automotive vehicles," *Vehicle System Dynamics,* vol. 46, no. 9, pp. 763-788, 2008.

[23] R. Zarringhalam, A. Rezaeian, W. Melek, A. Khajepour, S. k. Chen, and N. Moshchuk, "A comparative study on identification of vehicle inertial parameters," in *2012 American Control Conference (ACC)*, 27-29 June 2012 2012, pp. 3599-3604, doi: 10.1109/ACC.2012.6314832.

[24] S. S. Haykin, *Kalman filtering and neural networks* (Adaptive and learning systems for signal processing, communications, and control). New York: Wiley, 2001, pp. xiii, 284 p.

[25] S. Hong, C. Lee, F. Borrelli, and J. K. Hedrick, "A Novel Approach for Vehicle Inertial Parameter Identification Using a Dual Kalman Filter," *IEEE Transactions on Intelligent Transportation Systems,* vol. 16, no. 1, pp. 151-161, 2015, doi: 10.1109/tits.2014.2329305.

[26] S. Hong, T. Smith, F. Borrelli, and J. K. Hedrick, "Vehicle inertial parameter identification using Extended and unscented Kalman Filters," in *16th International IEEE Conference on Intelligent Transportation Systems (ITSC 2013)*, 6-9 Oct. 2013 2013, pp. 1436-1441, doi: 10.1109/ITSC.2013.6728432.

[27] C. Li, Y. Liu, L. Sun, Y. Liu, M. Tomizuka, and W. Zhan, "Dual Extended Kalman Filter Based State and Parameter Estimator for Model-Based Control in Autonomous Vehicles," presented at the 2021 IEEE International Intelligent Transportation Systems Conference (ITSC), 2021.

[28] X. Huang and J. Wang, "Real-Time Estimation of Center of Gravity Position for Lightweight Vehicles Using Combined AKF–EKF Method," *IEEE Transactions*

doi:10.6342/NTU202403171

on Vehicular Technology, vol. 63, no. 9, pp. 4221-4231, 2014, doi: 10.1109/tvt.2014.2312195.

[29] C. Cheng and D. Cebon, "Parameter and state estimation for articulated heavy vehicles," *Vehicle System Dynamics,* vol. 49, no. 1-2, pp. 399-418, 2011/02/01 2011, doi: 10.1080/00423110903406656.

[30] T. Kailath, A. H. Sayed, and B. Hassibi, *Linear estimation* (Prentice Hall information and system sciences series). Upper Saddle River, N.J.: Prentice Hall, 2000, pp. xxvi, 854 p.

[31] T. A. Wenzel, K. J. Burnham, M. V. Blundell, R. A. Williams, and A. Fairgrieve, "Simplified extended Kalman filter for automotive state estimation," *International Journal of Modelling, Identification and Control,* vol. 3, no. 3, pp. 201-211, 2008, doi: 10.1504/ijmic.2008.02012.

[32] S. J. Julier, J. K. Uhlmann, and H. F. Durrant-Whyte, "A new approach for filtering nonlinear systems," in *Proceedings of 1995 American Control Conference-ACC'95*, 1995, vol. 3: IEEE, pp. 1628-1632.

[33] E. A. Wan and R. Van Der Merwe, "The unscented Kalman filter for nonlinear estimation," in *Proceedings of the IEEE 2000 adaptive systems for signal processing, communications, and control symposium (Cat. No. 00EX373)*, 2000: Ieee, pp. 153-158.

[34] T. Zhu and H. Zheng, "Application of unscented Kalman filter to vehicle state estimation," in *2008 ISECS International Colloquium on Computing, Communication, Control, and Management*, 2008, vol. 2: IEEE, pp. 135-139.

[35] M. Karasalo and X. Hu, "An optimization approach to adaptive Kalman filtering," *Automatica,* vol. 47, no. 8, pp. 1785-1793, 2011.

[36] H. Eric Tseng, L. Xu, and D. Hrovat, "Estimation of land vehicle roll and pitch angles," *Vehicle System Dynamics,* vol. 45, no. 5, pp. 433-443, 2007, doi: 10.1080/00423110601169713.

[37] L. Imsland, H. F. Grip, T. A. Johansen, T. I. Fossen, J. C. Kalkkuhl, and A. Suissa, "Nonlinear observer for vehicle velocity with friction and road bank angle adaptation-validation and comparison with an extended Kalman filter," SAE Technical Paper, 0148-7191, 2007.

doi:10.6342/NTU202403171

[38] J. Stephant, A. Charara, and D. Meizel, "Virtual sensor: Application to vehicle sideslip angle and transversal forces," *IEEE Transactions on industrial electronics,* vol. 51, no. 2, pp. 278-289, 2004.

[39] S. Melzi and E. Sabbioni, "On the vehicle sideslip angle estimation through neural networks: Numerical and experimental results," *Mechanical Systems and Signal Processing,* vol. 25, no. 6, pp. 2005-2019, 2011.

[40] F. Cheli, E. Sabbioni, M. Pesce, and S. Melzi, "A methodology for vehicle sideslip angle identification: comparison with experimental data," *Vehicle System Dynamics,* vol. 45, no. 6, pp. 549-563, 2007.

[41] Y. Liu, D. Cui, and W. Peng, "Moving horizon estimation of vehicle state and parameters," *Journal of Vibroengineering,* vol. 25, no. 2, pp. 409-427, 2022, doi: 10.21595/jve.2022.22795.

[42] A. Gelb, *Applied optimal estimation*. MIT press, 1974.

[43] R. E. Kalman, "A new approach to linear filtering and prediction problems," 1960.

[44] G. Welch and G. Bishop, "Welch & Bishop , An Introduction to the Kalman Filter 2 1 The Discrete Kalman Filter In 1960," 1994.

[45] L. Nelson and E. Stear, "The simultaneous on-line estimation of parameters and states in linear systems," *IEEE Transactions on automatic Control,* vol. 21, no. 1, pp. 94-98, 1976.

[46] *SAE J670 Vehicle Dynamics Terminology*, 1952, 2022.

[47] I. The MathWorks, "Vehicle Dynamics Blockset R2024a," ed: The MathWorks, Inc., 2024.

[48] A. B. Will and S. H. Z˚Ak, "Modelling and Control of an Automated Vehicle," *Vehicle System Dynamics,* vol. 27, no. 3, pp. 131-155, 1997, doi: 10.1080/00423119708969326.

[49] H. B. Pacejka, "Tire and Vehicle Dynamics, 3rd Edition," (in English), *Tire and Vehicle Dynamics, 3rd Edition,* pp. 1-632, 2012. [Online]. Available: <Go to ISI>://WOS:000322044900016.

[50] "dSPACE ASM," ed: dSPACE GmbH, 2024.

[51] X. Niu, Y. Ban, Q. Zhang, T. Zhang, H. Zhang, and J. Liu, "Quantitative Analysis to the Impacts of IMU Quality in GPS/INS Deep Integration," *Micromachines,* vol. 6, no. 8, pp. 1082-1099, 2015, doi: 10.3390/mi6081082.

doi:10.6342/NTU202403171

[52] *ISO 3888-1:2018 Passenger cars — Test track for a severe lane-change manoeuvre — Part 1: Double lane-change*, 2018.

[53] A. Renski, "Identification of driver model parameters," *Int J Occup Saf Ergon,* vol. 7, no. 1, pp. 79-90, 2001, doi: 10.1080/10803548.2001.11076478.

[54] *ISO 4138:2021 Passenger cars — Steady-state circular driving behaviour — Open-loop test methods*, 2021.

doi:10.6342/NTU202403171

Appendix A

MATLAB/Simulink simulation

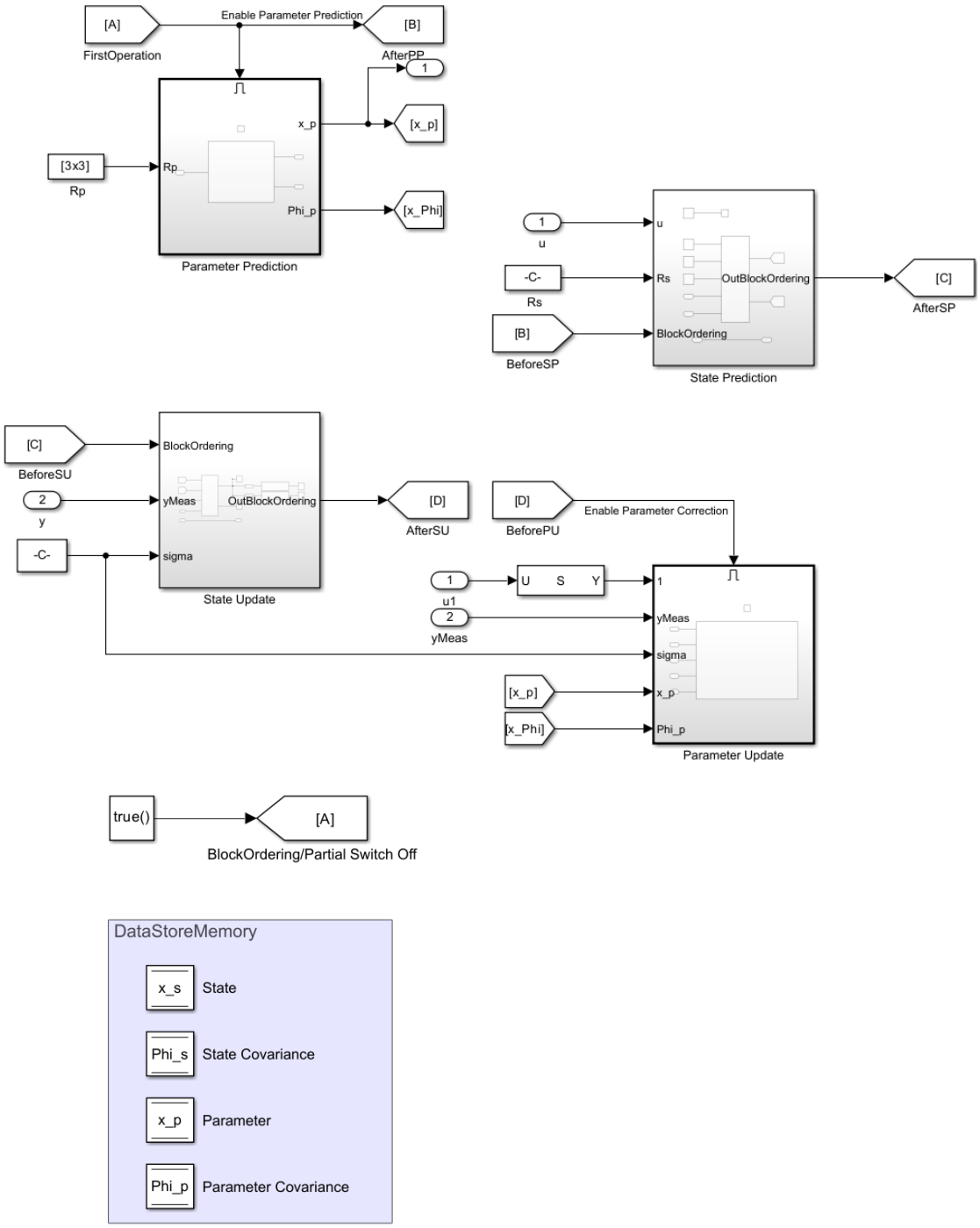

doi:10.6342/NTU202403171

Appendix B

Fixed vehicle parameters

Parameter	Value	Unit
l	2.7	m
c	$l-b$	m
g	9.81	m/s^2
r	0.35	m
t_f	1.54	m
t_r	1.54	m
μ	150	kg
m_s	$m-\mu$	kg
κ_ϕ	58000	N∗ m/rad
β_ϕ	8000	N∗ m/(rad/s)
h	h_s+r	m

Parameters for longitudinal slip

Shape factor C	p_{Cx1}	1.579
Peak factor D	p_{Dx1}	1.0422
	p_{Dx2}	-0.0827
	p_{Dx3}	0
Curvature factor E	p_{Ex1}	0.11185
	p_{Ex2}	0.3127
	p_{Ex3}	0
	p_{Ex4}	0.001603
Slip stiffness BCD	p_{Kx1}	21.69
	p_{Kx2}	13.774
	p_{Kx3}	-0.4119
Horizontal shift H	p_{Hx1}	0.000216
	p_{Hx2}	0.001154
Vertical shift V	p_{Vx1}	0.000016
	p_{Vx2}	0.000104

doi:10.6342/NTU202403171

Parameters for pure lateral slip

Shape factor C	p_{Cy1}	1.3332
Peak factor D	p_{Dy1}	0.8784
	p_{Dy2}	-0.06445
	p_{Dy3}	0
Curvature factor E	p_{Ey1}	-0.8227
	p_{Ey2}	-0.6062
	p_{Ey3}	0.09825
	p_{Ey4}	0
Slip stiffness BCD	p_{Ky1}	-15.314
	p_{Ky2}	1.7044
	p_{Ky3}	0.36986
Horizontal shift H	p_{Hy1}	-0.001804
	p_{Hy2}	0.003518
	p_{Hy3}	0
Vertical shift V	p_{Vy1}	-0.001804
	p_{Vy2}	0.003518
	p_{Vy3}	0

doi:10.6342/NTU202403171

Parameters for pure aligning torque

Shape factor C	p_{Cy1}	1.3332
Peak factor D	p_{Dy1}	0.8784
	p_{Dy2}	-0.06445
	p_{Dy3}	0
Curvature factor E	p_{Ey1}	-0.8227
	p_{Ey2}	-0.6062
	p_{Ey3}	0.09825
	p_{Ey4}	0
Slip stiffness BCD	p_{Ky1}	-15.314
	p_{Ky2}	1.7044
	p_{Ky3}	0.36986
Horizontal shift H	p_{Hy1}	-0.001804
	p_{Hy2}	0.003518
	p_{Hy3}	0
Vertical shift V	p_{Vy1}	-0.001804
	p_{Vy2}	0.003518
	p_{Vy3}	0

Additional mass load 1

Mass load 1

1500 **[kg]**

Center of gravity load 1

x	y	z	
-1.5	0	1	**[m]**

Inertia tensor load 1 **[kg*m2]**

	x	y	z
x	125	0	0
y	0	625	0
z	0	0	625

doi:10.6342/NTU202403171

Additional mass load 2

Mass load 2

500	[kg]

Center of gravity load 2

x	y	z	
-1.5	0	1	[m]

Inertia tensor load 2 [kg*m2]

	x	y	z
x	80	0	0
y	0	200	0
z	0	0	200

doi:10.6342/NTU202403171